Available online at www.sciencedirect.com
ScienceDirect
International Journal of Plasticity 24 (2008) 1481–1515
INTERNATIONAL JOURNAL OF Plasticity
www.elsevier.com/locate/ijplas

# Benchmark experiments and characteristic cyclic plasticity deformation

Yanyao Jiang *, Jixi Zhang

*University of Nevada, Department of Mechanical Engineering (312), Reno, NV 89557, USA*

Received 3 June 2007; received in final revised form 17 October 2007
Available online 3 December 2007

**Abstract**

Key issues in cyclic plasticity modeling are discussed based upon representative experimental observations on several commonly used engineering materials. Cyclic plasticity is characterized by the Bauschinger effect, cyclic hardening/softening, strain range effect, nonproporitonal hardening, and strain ratcheting. Additional hardening is identified to associate with ratcheting rate decay. Proper modeling requires a clear distinction among different types of cyclic plasticity behavior. Cyclic hardening/softening sustains dependent on the loading amplitude and loading history. Strain range effect is common for most engineering metallic materials. Often, nonproportional hardening is accompanied by cyclic hardening, as being observed on stainless steels and pure copper. A clarification of the two types of material behavior can be made through benchmark experiments and modeling technique. Ratcheting rate decay is a common observation on a number of materials and it often follows a power law relationship with the number of loading cycles under the constant amplitude stress controlled condition. Benchmark experiments can be used to explore the different cyclic plasticity properties of the materials. Discussions about proper modeling are based on the typical cyclic plasticity phenomena obtained from testing several engineering materials under various uniaxial and multiaxial cyclic loading conditions. Sufficient experimental evidence points to the unambiguous conclusion that none of the hardening phenomena (cyclic hardening/softening, strain range effect, nonproportional hardening, and strain hardening associated with ratcheting rate decay) is isotropic in nature. None of the hardening behavior can be properly modeled with a change in the yield stress.


*Keywords:* Cyclic plasticity; Cyclic hardening/softening; Non-masing behavior; Nonproportional hardening; Ratcheting

* Corresponding author. Tel.: +1 775 784 4510; fax: +1 775 784 1701.
*E-mail address:* yjiang@unr.edu (Y. Jiang).

0749-6419/$ - see front matter © 2007 Elsevier Ltd. All rights reserved.
doi:10.1016/j.ijplas.2007.10.003

## 1. Introduction

Cyclic plasticity deals with the nonlinear stress–strain response of a material subjected to repeated external loading. Most load bearing components in engineering are subjected to cyclic loading, and cyclic plastic deformation of the materials is unavoidable. The elastic–plastic stress–strain response plays a pivotal role in the design and failure analyses of engineering components. Despite extensive work that has been conducted on cyclic plasticity, many questions and difficulties exist. Accurate modeling of cyclic plasticity is still difficult. The relationship between the macroscopic cyclic plastic deformation and the microscopic mechanisms remains qualitative in nature.

Typical cyclic plastic deformation phenomena include the Bauschinger effect, cyclic hardening/softening, Masing and non-Masing behavior (strain range effect), nonproportional hardening, and cyclic strain ratcheting deformation. Plasticity models or constitutive equations are mathematical relations describing the stress–strain response of a material subjected to external loading. The theory of plasticity is a part of the broad and fascinating subject of mechanics of materials or continuum mechanics, which spans the spectrum from the fundamental aspects of elastic and inelastic behavior to the practical solution of engineering problems. Due to the great complication involved in cyclic plastic deformation, most of the existing theories have limited capabilities to properly describe the experimentally observed cyclic plasticity phenomena.

Despite the possible claims of the plasticity theories based upon the first principles, it is safe to say that all the existing theories that can possibly describe the macroscopic cyclic plasticity behavior are phenomenological in nature. This is particularly true for those dealing with polycrystalline engineering materials. The phenomenological models are the mathematical description based upon the limited observations of the experimental phenomena. For any phenomenological modeling, it is impossible to prove theoretically the correctness of a model. The general practice is to use the experimental cyclic stress–strain response to support the appropriateness of a theory. However, it is possible to theoretically and experimentally prove that a theory is wrong or inappropriate. Particularly, benchmark experiments can be conducted and the results can be used to critically evaluate a cyclic plasticity theory.

It is difficult to describe the detailed hysteresis loops and their evolution even under uniaxial loading for the practically homogeneous and initially isotropic engineering materials. For example, the transient behavior under multiple-step high–low sequence loading is difficult to describe for such materials as stainless steels and pure copper. It was found that the long-term ratcheting behavior under uniaxial loading was very difficult to simulate for stainless steels (Chaboche and Nouailhas, 1989; Chaboche, 1991).

The overall objective of the current work is to provide fundamental cyclic plasticity phenomena observed experimentally to better understand cyclic plasticity. It is aimed at serving as a guideline for the development of constitutive relations for cyclic plasticity. The discussions will be helpful for the critical evaluation of an existing model. The concentration will be placed on the macroscopic phenomena based on continuum mechanics with polycrystalline materials under cyclic loading near the room temperature. A basic implicit assumption in macroscopic continuum mechanics is that a material point is small enough so that it can be treated as a mathematical point but it is large enough to contain at least several grains so that the material can be treated as being homogeneous. General discussions will be made with respect to the proper modeling for describing the observed cyclic plastic deformation behavior.

## 2. Bauschinger effect

Baushinger effect is a fundamental and well known cyclic plasticity behavior. For the sake of completeness, the Bauschinger effect will be discussed briefly. According to a "standard" definition, the Bauschinger effect is "the phenomenon by which plastic deformation increases yield strength in the direction of plastic flow and decreases it in other direction" (Metals Reference Book, 1993). The Bauschinger effect is schematically described in Fig. 1 using an idealized material under uniaxial loading. If the yield stress is $\sigma_0$, plastic deformation occurs when the stress exceeds $\sigma_0$ the first time for a virgin material. When loading is reversed, the material will display elastic deformation until the difference between the current stress and the stress at which the load started to reverse reaches $2\sigma_0$. Due to work hardening, the stress at which yielding occurs in the reversed direction is lower than $\sigma_0$.

It can be deduced according to the Bauschinger effect that cyclic plasticity in a loading cycle can develop under zero-to-tension uniaxial loading. Fig. 2 shows the experimentally obtained stress–strain hysteresis loops of 1070 steel under zero-to-tension uniaxial loading.

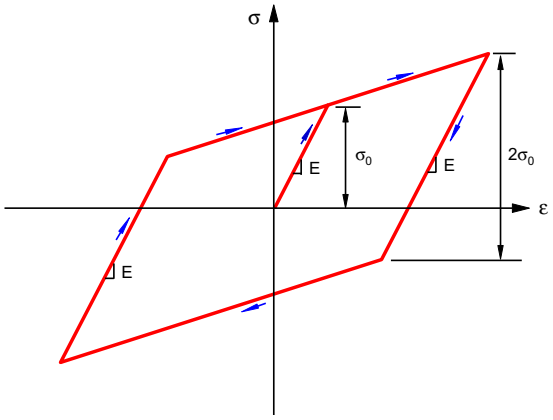


Fig. 1. Schematic illustration of the Bauschinger effect.

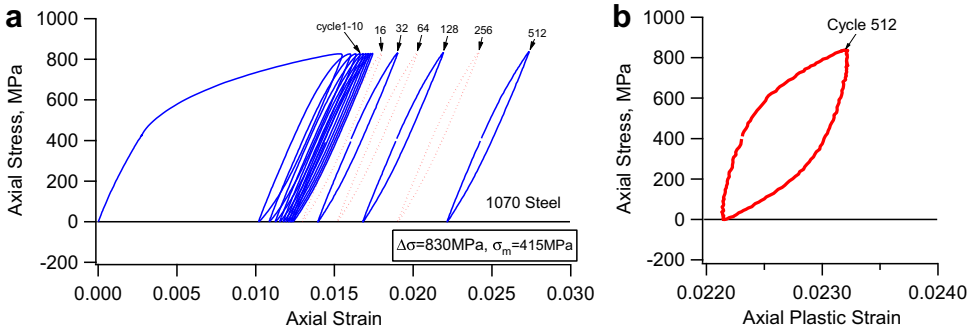


Fig. 2. 1070 steel under zero-to-tension uniaxial loading: (a) stress–strain hysteresis loops and (b) stress–plastic strain hysteresis loop for a selected loading cycle (Jiang, 1993).

The stress range ($\Delta\sigma$) was 830 MPa and the mean stress ($\sigma_m$) was 415 MPa. The stress controlled experiment resulted in ratcheting deformation which will be discussed in a later section. Since creep is minimal for 1070 steel at room temperature, the result shown in Fig. 2 clearly indicates that cyclic plasticity develops under zero-to-tension loading. The stress–plastic strain hysteresis loop shown in Fig. 2b for a selected loading cycle suggests that the "real" yield stress for the high carbon steel under cyclic loading is much lower than the value that most people would use for modeling the cyclic plasticity of the material.

The traditional modeling of cyclic plasticity using a yield surface warrants the consideration of the Bauschinger effect.

## 3. Cyclic hardening and softening

Cyclic hardening/softening refers to the hardening or softening response of a material subjected to repeated loading. It is often reflected by testing the material under fully reversed strain-controlled loading. With a controlled strain amplitude, a material is cited to display cyclic hardening/softening when the stress amplitude increases/decreases with increasing loading cycle. Fig. 3 shows the stress–strain hysteresis loops of representative loading cycles obtained from testing an annealed OFHC polycrystalline copper under fully reversed strain-controlled uniaxial loading (Zhang, 2004). The axial strain amplitude ($\Delta\varepsilon/2$) was 0.3%. Significant cyclic hardening is observed.

Most materials display cyclic hardening or softening. Some materials, such as the stainless steels and pure copper, exhibit very significant cyclic hardening while some other materials display less significant hardening or softening. A "rule-of-thumb" is that a hard material cyclically softens and a soft material cyclically hardens. This is evident in pure copper and high strength steels (Doong et al., 1990; Boller and Seeger, 1987).

### *3.1. Cyclic hardening or softening is not only dependent on the material but also on the loading magnitude and loading history*

A typical example is the stainless steel AISI 304. Cyclic hardening and softening can be identified by checking the variation of the stress amplitude with the loading cycles under

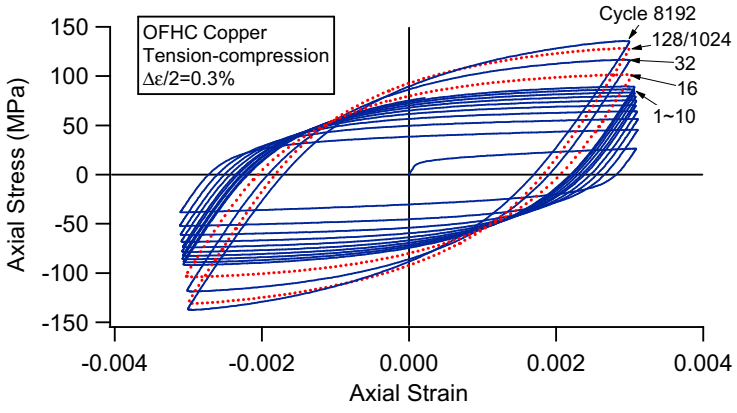


Fig. 3. Representative stress–strain hysteresis loops of an OFHC copper under fully reversed strain-controlled uniaxial loading ($\Delta\varepsilon/2 = 0.3\%$) (Zhang, 2004).

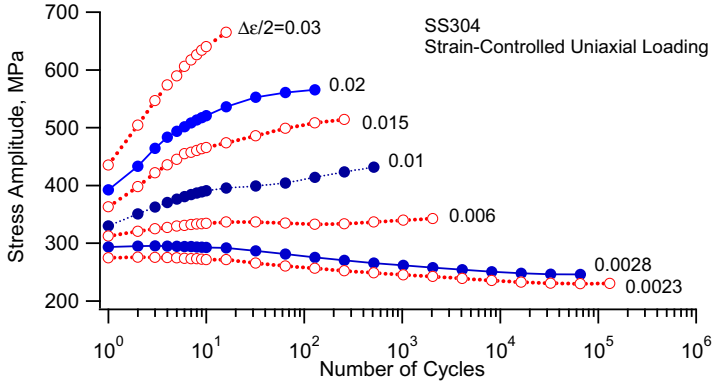


Fig. 4. Variation of the stress amplitude with the loading cycles for fully reversed strain-controlled uniaxial loading of stainless steel 304 (Jiang and Kurath, 1997a).

the strain-controlled loading condition (Fig. 4). The material displays significant cyclic hardening when the strain amplitude is higher than 1%. At a strain amplitude of approximately 0.5%, the stress amplitude does not change much with the increase in loading cycle. At a strain amplitude of 0.28% or lower, the material displays cyclic softening.

The dependence of cyclic hardening/softening behavior on the loading history can be seen from the results shown in Fig. 5. Fig. 5a shows the stress amplitude as a function of the loading cycles at a strain amplitude of 0.6% for the stainless steel 304 under fully reversed loading. The open circles represent the results obtained from a single-step constant amplitude loading, which is identical to one curve shown in Fig. 4. The other curve in Fig. 5a was the results of the second loading step in a high–low two-step loading history. The first step had a strain amplitude of 3% and it lasted for 10 cycles. The second step had a strain amplitude of 0.6% and it lasted for more than 2000 cycles before fatigue failure occurred. Clearly, the material displayed cyclic hardening in the single-step constant amplitude loading. However, with a higher loading amplitude prior loading history, the second step loading in the high–low loading sequence displayed significant cyclic softening.

Fig. 5b shows the results of the two loading scenarios similar to those in Fig. 5a. An OFHC copper was subjected to a strain amplitude of 0.2% under fully reversed tension–compression loading with and without a prior loading history. The curve with open circles represents the results from a single-step test. Significant cyclic hardening followed by saturation was observed. The curve with solid circles in Fig. 5b represents the results with a prior loading history which had a strain amplitude of 1% for 130 cycles. In the second step loading with a strain amplitude of 0.2%, cyclic softening occurred and the saturation stress amplitude was recovered to that from a single-step test.

### *3.2. Cyclic hardening/softening is not isotropic behavior*

If the loading amplitude is increased or decreased after cyclic saturation at a constant loading amplitude, cyclic hardening/softening may take place again until a new saturation state is established. In this sense, cyclic hardening/softening is not a transient behavior – it

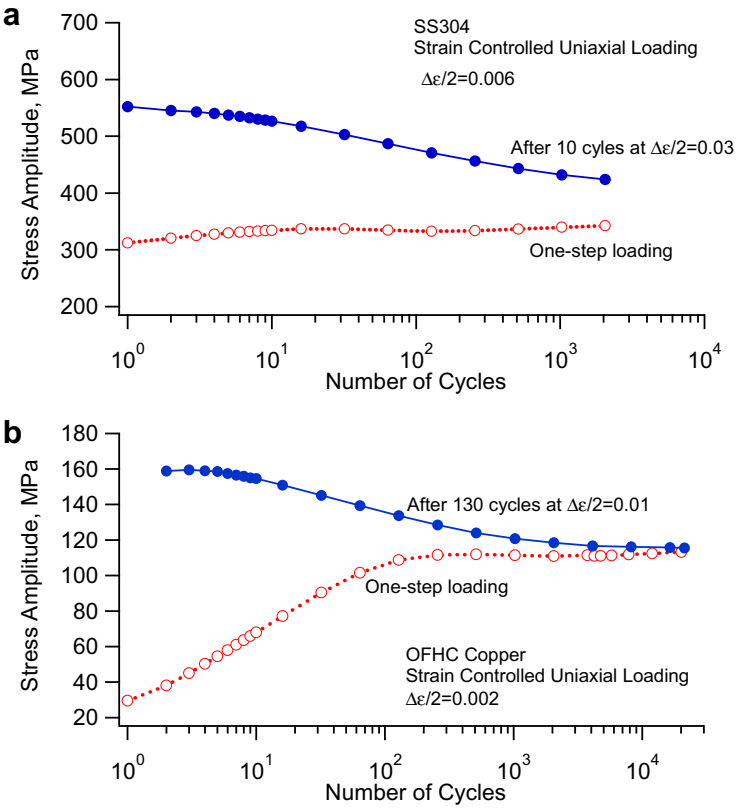


Fig. 5. Dependence of cyclic softening on loading history: (a) SS304 and (b) OFHC copper (Zhang, 2004).

persists. The persistent cyclic hardening/softening is evident from the stress results obtained from the three-step strain-controlled sequence loading on stainless steel 304 (Fig. 6). The material was subjected to fully reversed strain-controlled uniaxial loading. The first step had a strain amplitude of 0.235%. After 130,000 loading cycles, the stress response stabilized. Cyclic softening was observed before stabilization. The same specimen was further loaded at a strain amplitude of 1.5% for 10 loading cycles in the second loading step. Significant cyclic hardening was observed. After the second loading step, the strain amplitude was returned to that of the first loading step (0.235%). The material was tested until fatigue failure after 62,000 cycles in the third loading step. Continuous cyclic softening was observed in Step 3. It should be noted that the cycle numbers are shifted in the figure for comparison. The results shown in Fig. 6 reveal that cyclic hardening occurred in the second loading step regardless of the stabilization of the stress response in the first loading step. Cyclic softening occurred again in the third loading step despite the long prior loading history. It is noticed again that with identical strain amplitudes in Step 1 and Step 3, the stress responses are different. The stress amplitude in Step 3 is significantly higher than that in Step 1. This is similar to the results shown in Fig. 5a. The specimen failed due to fatigue after 62,000 loading cycles in Step 3.

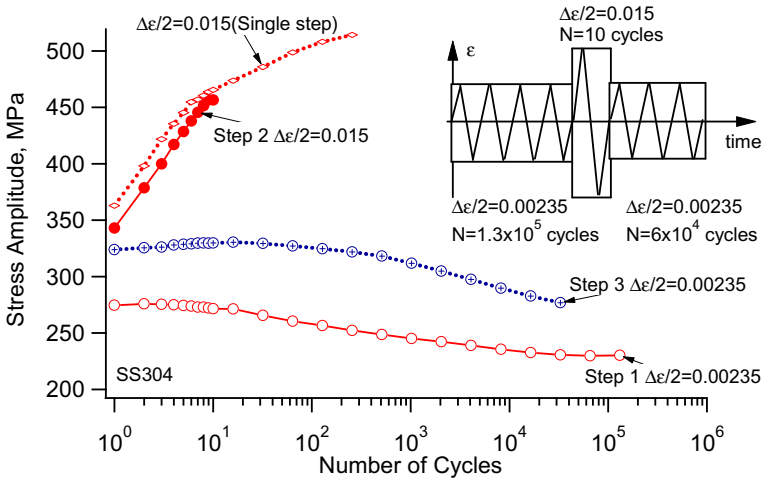


Fig. 6. Stress amplitude variation with number of loading cycles in each loading step in a three-step fully reversed strain-controlled loading sequence (Jiang and Kurath, 1997a).

The dotted curve with open markers in Fig. 6 was the results of the stress amplitude under single-step strain-controlled constant amplitude loading. The influence of the prior loading on cyclic hardening behavior can be also found by comparing the stress response of the single-step loading at a strain amplitude of 0.015 with that in the second step of the three-step sequence loading in Fig. 6.

The persistent cyclic hardening/softening phenomenon observed from the multiple-step loading experiments can lead to the conclusion that modeling of cyclic hardening and softening cannot use the isotropic hardening concept. If cyclic hardening/softening is an isotropic property, no further cyclic hardening/softening would occur after the material has been stabilized. Accordingly, the material should have displayed stabilized cyclic plastic deformation after being stabilized in the first loading step.

### 3.3. Cyclic hardening/softening cannot be modeled by using the change of the yield stress

A careful observation of the stress–strain hysteresis loops will help identify the characteristics of cyclic hardening/softening. The presentation will use the stress range versus the plastic strain range in the semi-log scale. The origin of the coordinates system is located at the lower or upper tip of the stress–plastic strain hysteresis loop (refer to the insert in Fig. 7). Use of a logarithmic scale on the plastic strain range axis affords insight into smaller plastic strain phenomena that are often lost when using a linear axis to plot larger plastic strain data.

Results shown in Fig. 7 were obtained from testing specimens under fully reversed strain-controlled uniaxial loading for an annealed OFHC copper under two strain amplitudes. The experiments were conducted using specimens without prior loading histories. The first reversal is modified to the range format by multiplying both the stress and plastic strain by two. This practice is carried for any presentations for the first reversals in this paper. A glance at Fig. 7 reveals that the material displays significant cyclic hardening under both strain amplitudes. It can be also observed that the stress–plastic strain hysteresis loops

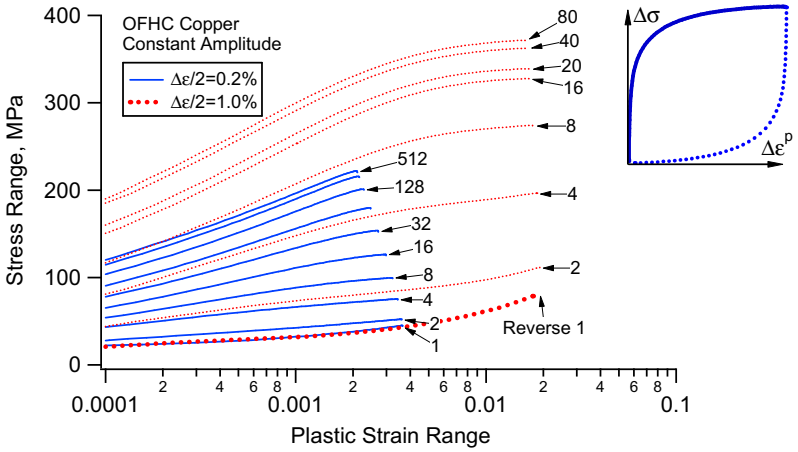


Fig. 7. Cyclic hardening of OFHC copper under fully reversed strain-controlled uniaxial loading.

are not "similar" in shape for different loading cycles under constant amplitude loading. The shapes of the loops corresponding to the initial loading cycles are noticeably different from those of the cycles near stabilization. The similarity of the stress–strain hysteresis loops can be better distinguished using the results obtained from testing a stainless steel.

Fig. 8 shows the deformation reflecting the evolution of the shapes of the stress–plastic strain loops under fully reversed strain-controlled uniaxial loading for stainless steel 304. Again, the results are shown in semi-log scale using the stress range and the plastic strain range. The experiments were conducted using the specimens without prior loading histories.

For the stainless steel, the stress controlled test with a smaller stress amplitude ($\Delta\sigma/2 = 250$ MPa) displays overall softening, evident by the increasing plastic strain with increasing number of cycles. If the test had been conducted in strain control, a cyclic dependent decrease in the stress amplitude would have been observed. However, the defor-

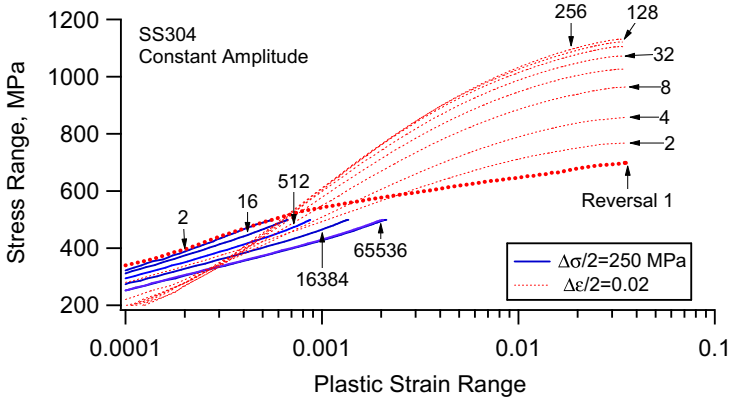


Fig. 8. Cyclic hardening/softening of stainless steel 304 under fully reversed uniaxial loading (Jiang and Kurath, 1997a).

mation behavior at smaller plastic strain amplitudes is more pronounced and experimentally quantifiable when stress controlled experiments are conducted. In contrast, the material under a larger stain amplitude ($\Delta\varepsilon/2 = 2.0\%$) exhibits overall cyclic hardening, evidenced by an increase in the stress amplitude with increasing number of cycles. These results are consistent with the behavior traditionally observed for fully reversed strain-controlled fatigue tests.

Despite the frequent use of the concept, there is no universally acceptable definition for the yield stress of the material in cyclic plasticity. It would be ideal to use the elastic limit since it is theoretically sound. However, the sensitivity of the elastic limit to the personal judgment may have prevented it from a general use. An offset concept would be more practical. Obviously, the 0.2% offset concept used in the definition of a pseudo yield stress in monotonic loading is not acceptable. This is because a plastic strain amplitude or range of 0.2% is not insignificant deformation for cyclic plasticity. On the other hand, a very small offset would have the same problem associated with the elastic limit. A practical offset limit can be related to the accuracy of the strain measurement. Most strain gages and strain gage based extensometers can reliably detect a strain of 10 $\mu\varepsilon$. A measurement of a strain of 100 $\mu\varepsilon$ can be easily achieved by most strain gages and strain gage based extensometers. In order to facilitate a discussion about the yield stress, an offset of 100 $\mu\varepsilon$ is assumed for stainless steel 304. With this in mind, it can be found that the offset yield stress of SS304 decreases with increasing number of loading cycles for both loading amplitudes shown in Fig. 8. It should be noticed that cyclic hardening was identified when the strain amplitude was 2%.

The results shown in Figs. 7 and 8 suggest that the cyclic hardening/softening cannot be characterized by using the change in the yield stress. If cyclic hardening/softening can be attributed to the change in the yield stress, all the stress–plastic strain hysteresis loops under constant amplitude loading should be "similar" in shape. "Similarity" here means that all the upper or lower branches of the stress–plastic strain hysteresis loops should match or fall in a master curve through a parallel shift of the reversals in the linear-log scale coordinates shown in Figs. 7 and 8, with the only difference being the yield stress among all the loops irrespective of the definition of the yield stress. Clearly, this is not the case for both materials shown in Figs. 7 and 8. For both materials under different loading amplitudes, the shape of the reversals changes with the number of loading cycle. Typically, fan-shaped reversals in the semi-log scale are observed under constant amplitude loading for most engineering materials that the authors have experienced.

In addition, the yield stress should increase with increasing loading cycles for a material displaying cyclic hardening if the yield stress can be used to characterize cyclic hardening. This is not true as shown in Fig. 8 for the strain-controlled experiment with a strain amplitude of 2%.

The detailed loops obtained from multiple-step loading can provide further evidence to support the conclusion drawn from the previous discussion. Fig. 9 shows the reversals taken from three loading steps in a low–high–low sequence loading experiment for the stainless steel 304. The stress amplitudes of the three loading steps have been shown in Fig. 6. In the linear-log scale, the reversals should be parallel if cyclic hardening/softening can be characterized by using the change of the yield stress. Clearly, the shapes of the reversals are not similar and they do not come together by shifting the reversals up or down in the linear-log scale. In Steps 2 and 3, the fan-shaped reversals are apparent. If an offset of 100 $\mu\varepsilon$ plastic strain range is used to define the yield stress again, it can be

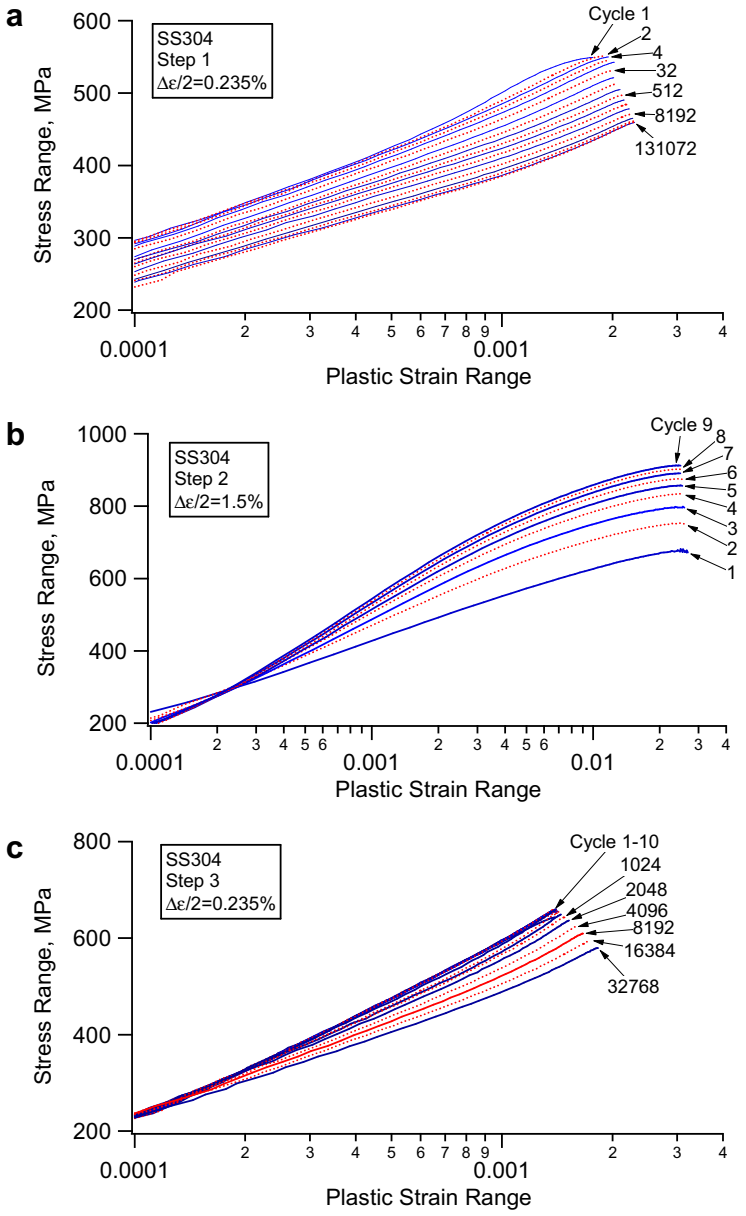


Fig. 9. Reversals taken from the three-step sequence loading for stainless steel 304 under fully reversed strain-controlled uniaxial loading (data identical to that in Fig. 6).

found that the second step loading with a large strain amplitude of 1.5% has a lower yield stress than that in the first and third loading steps where the strain amplitude was 0.235%.

It is worthwhile to point out that the cyclic softening should be differentiated from a localized cyclic plastic deformation phenomenon occurring in materials displaying Lüders

band during yielding (Jiang, 2001; Zhang and Jiang, 2004). The Lüders band propagation typically occurs in carbon steels under cyclic loading, resulting in an overall cyclic softening.

## 4. Masing behavior and strain range effect

### 4.1. Masing behavior

In a practical term, Masing behavior refers to the phenomenon that the ascending parts of the hysteresis loops obtained at different strain amplitudes are the same. A schematic illustration of Masing behavior is shown in Fig. 10. When the stress–plastic strain hysteresis loops under different strain amplitudes are presented with the lowers tips being tied together, the upper branches of the loops can follow an identical master curve.

Some engineering materials display Masing behavior under certain conditions. Fan and Jiang (2004) observed Masing behavior of a pressure vessel steel at 300 °C and 420 °C. Maier et al. (2006) observed Masing behavior of an ultra-fine grained copper. Christ and Mughrabi (1996) tested copper polycrystals using a special incremental step test that led to constancy in the microstructure. Masing behavior was observed. Wang and Laird (1988) found that a polycrystalline copper showed Masing behavior under ramp loading. Raman and Padmanabhan (1996) pointed out that Masing behavior can be observed in 304LN stainless steel which had been cold worked for 30% prior testing. Plumtree and Abdel-Raouf (2001) conducted a series of fully reversed cyclic strain tests on a range of ferrous and non-ferrous metals. It was observed that metals with finely dispersed particles and single phase low stacking fault metals exhibited Masing behavior. For high stacking fault energy metals where the cyclic deformation was matrix controlled, the cyclic stress–strain response was non-Masing. However, Masing behavior was observed below a threshold strain level. Above the threshold, non-Masing behavior occurred, which was accompanied with the formation of a dislocation cellular microstructure.

From a microscopic viewpoint, Masing behavior indicates that the microstructures are stable against fatigue-induced changes (Maier et al., 2006). For nickel-based superalloy PM 1000, the strong influence of the dispersoids on dislocation mobility in combination with the constancy of dislocation arrangement yields Masing behavior for the incremental

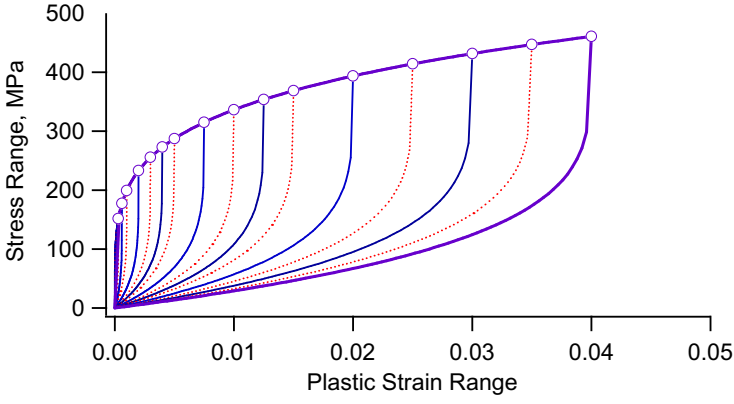


Fig. 10. Schematic illustration of Masing behavior.

step tests (Heilmaier et al., 2000). Copper single crystals exhibit Masing behavior if the current load is lower than the previous load. This implies that the previously established microstructures are capable of supporting the deformation specified at the current load amplitude (Li and Laird, 1993; Jameel et al., 2001).

*4.1.1. Most metallic materials exhibit non-Masing behavior*

Fig. 11 show the experimentally obtained stress–plastic strain hysteresis loops under fully reversed uniaxial loading for three different materials. All the experiments were conducted at room temperature. The loops represent the stabilized stress–strain response under the given loading amplitude. For a given material, all the stress–plastic strain hysteresis loops are tied together at the lower tips. AL-6XN is a super-austenitic stainless steel (Kalnaus and Jiang, 2007) and 16MnR is a pressure vessel steel (Gao et al., submitted for

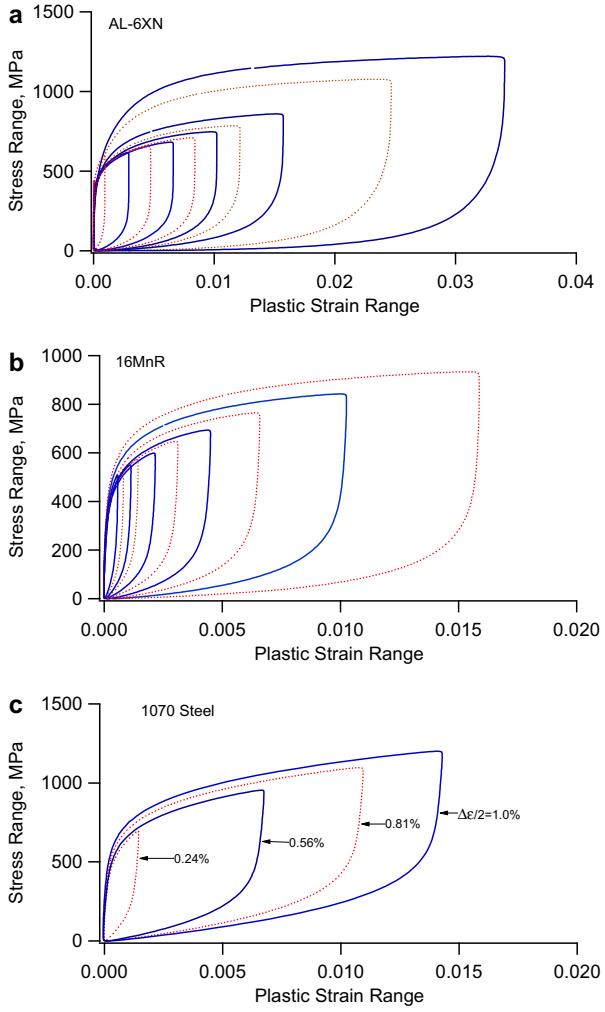


Fig. 11. Stabilized stress–plastic strain hysteresis loops with the lower tips tied together: (a) AL-6XN (Kalnaus and Jiang, 2007); (b) 16MnR (Gao et al., submitted for publication) and (c) 1070 Steel (Jiang, 1993).

publication). Clearly, non-Masing behavior is dependent on the material as well as the loading amplitude. Non-Masing behavior is more significant when the loading amplitude is large.

A better way to discuss non-Masing behavior is to use the reversals (branches) of the stress–plastic strain hysteresis loops (Fig. 12). The reversals (upper branches of the loops)

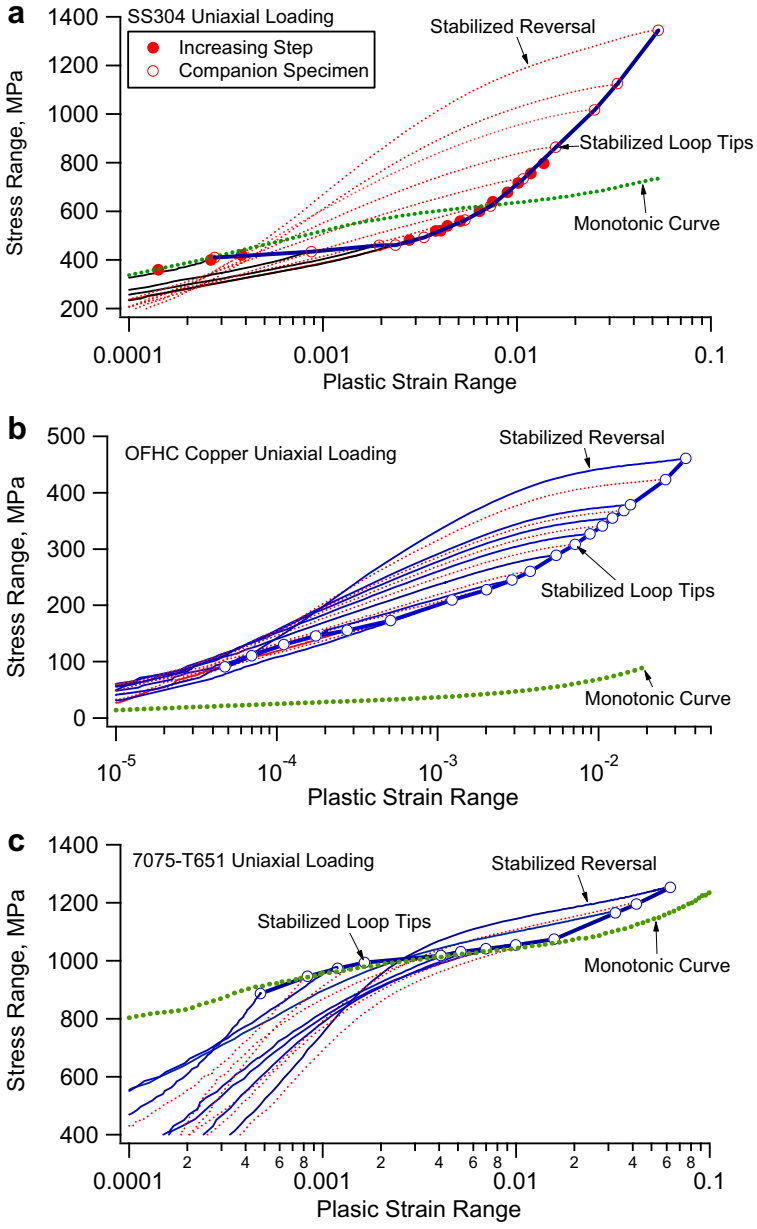


Fig. 12. Reversals from the stabilized stress–plastic strain hysteresis loops: (a) SS304 (Jiang and Kurath, 1997a); (b) OFHC copper and (c) 7075-T651.

after stabilization are presented in the form of the stress range versus the plastic strain range in the linear-log scale for three different materials. If a material displays Masing behavior, all the reversals should coincide.

The results shown in Fig. 12 clearly indicate that *the strain range effect or non-Masing behavior cannot be described by using the change of the yield stress*. As was previously discussed, a change in the yield stress can be reflected in the linear-log scale in Fig. 12 with a parallel shift of the curves in the vertical direction. The fan-shaped reversals shown in Fig. 12 for the three different materials suggest that the shapes of the stress–plastic strain hysteresis loops are different depending on the loading amplitude. In Fig. 12a, the experimental results obtained from the increasing step test coincided with that obtained from the companion specimens. In an increasing step test, one specimen was used and it was cycled to a stabilized state at each amplitude before increasing the amplitude to the next level. A companion specimen was cycled at constant amplitude until failure.

*4.1.2. A power law does not describe well the stress–strain relationship*

It is worthwhile to mention that the power law (Ramberg–Osgood) relationship does not describe well the stress–strain hysteresis loops nor the cyclic stress–strain curves. Regenerating Fig. 12a using the log–log scale for the results, Fig. 13 reveals that neither the branches of the loops nor the cyclic stress–strain curve are straight lines in the log–log scale. Therefore, the relationship of the stress and the plastic strain does not follow the power law relationship. It is noticed that part of the cyclic stress–strain curve with the plastic strain range being larger than 0.003 can be approximated by a straight line or a power law relationship. However, the branches of the stress–plastic strain hysteresis loops cannot be properly described using a power law relationship when the plastic strain range is larger than 0.003 for the material. The conclusion holds for the other two materials presented in Fig. 12 and several other materials including 1070 steel (Jiang and Kurath, 1997a), AL6XN stainless steel (Kalnaus and Jiang, 2007), 16MnR pressure vessel steel (Gao et al., submitted for publication), 1045 steel (Jiang, 2007), and stainless steel 304 L (Jiang, 2007).

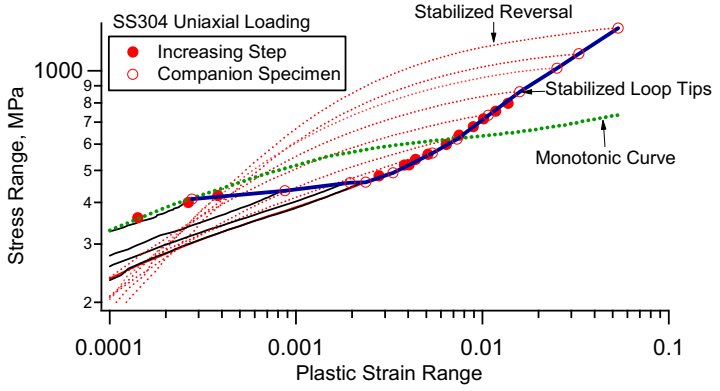


Fig. 13. Reversals of stainless steel 304 under uniaxial loading shown in log–log scale (Jiang and Kurath, 1997a).

### 4.2. High–low sequence loading

When dealing with the strain–range effect, a critical question is whether the stabilized stress–strain response is loading history dependent. Early modeling effort made by Chaboche et al. (1979) assumed isotropic behavior which implies that stabilized stress–strain response is loading history dependent. If a high–low sequence loading is conducted, the isotropic behavior assumes that prior high loading history will alter the *stabilized* stress–strain hysteresis loop of the subsequent lower loading as compared to that without a prior loading history. Later efforts by Ohno (1982) and McDowell (1985a) made use of a kinematic concept which implies a possible full recoverability of the stabilized stress–strain response irrespective of the prior loading history. Since the experimental results speak louder, discussions will be made based on the experimental observations on two materials subjected to two-step high–low sequence loading.

In a high–low loading sequence, a specimen is subjected to a high constant amplitude strain (or stress) until saturation. This is followed by constant amplitude loading with a lower stress or strain amplitude. If the stabilized stress–strain response in the second loading step (lower amplitude) is practically identical to that obtained with identical (to the lower amplitude) amplitude but without a prior loading history, the material is said to display a reversibility of deformation. Research on polycrystalline materials provides inconclusive results in terms of the reversibility of the material deformation (Feltner and Laird, 1967a; Pratt, 1967; Jiang and Kurath, 1997a).

Holzwarth and Ebmann (1994) and Watanabe et al. (2002) investigated the reversibility of stress amplitude and dislocation evolution in a single crystal copper oriented for single slip subjected to a high–low loading sequence. After saturation at a high strain amplitude larger than that in the plateau region of the cyclic stress–strain curve, the strain amplitude was changed to a value in the plateau region. The stress amplitude can be resumed to the level of the plateau region. Feltner and Laird (1967a,b) and Pratt (1967) observed a similar phenomenon in a polycrystalline copper.

Fig. 14 shows the results of three companion specimens subjected to identical pure shear loading at a shear strain amplitude ($\Delta\gamma/2$) of 0.315% for the study of the reversibility of stress response and dislocation substructure (Zhang and Jiang, 2005). The material was a textured OFHC polycrystalline copper. The three tubular specimens had different prior loading history before the constant amplitude loading. To set up the base for comparison, one specimen was subjected to the pure shear loading without a prior loading history (Constant Amplitude). One specimen was subjected to a prior loading history of cyclic torsion at $\Delta\gamma/2 = 2.1\%$ (Large Torsion) for 130 loading cycles. The third specimen had a 90° out-of-phase axial-torsion nonproportional loading (NPP Loading) history at $\Delta\varepsilon/2 = 0.3\%$ and $\Delta\gamma/2 = 0.52\%$ for 130 cycles prior to the pure torsion. Both specimens with prior loading histories experienced cyclic torsion at $\Delta\gamma/2 = 0.315\%$ for $6.5 \times 10^4$ cycles in Step 2. For the two specimens subjected to two-step high–low sequence loading, the saturated stress amplitudes in Step 2 were practically identical to that under the constant amplitude loading with the same strain amplitude (Fig. 14a). However, an examination of hysteresis loops using the stress range versus plastic strain range in the logarithmic scale (Fig. 14b) indicates that the stress difference at the low plastic strain region was significant. It is apparent that a prior large loading history practically had no influence on the saturated stress amplitude in Step 2, but had influence on the shape of hysteresis loop. TEM observations revealed that a part of dislocation cells formed at the high strain ampli-

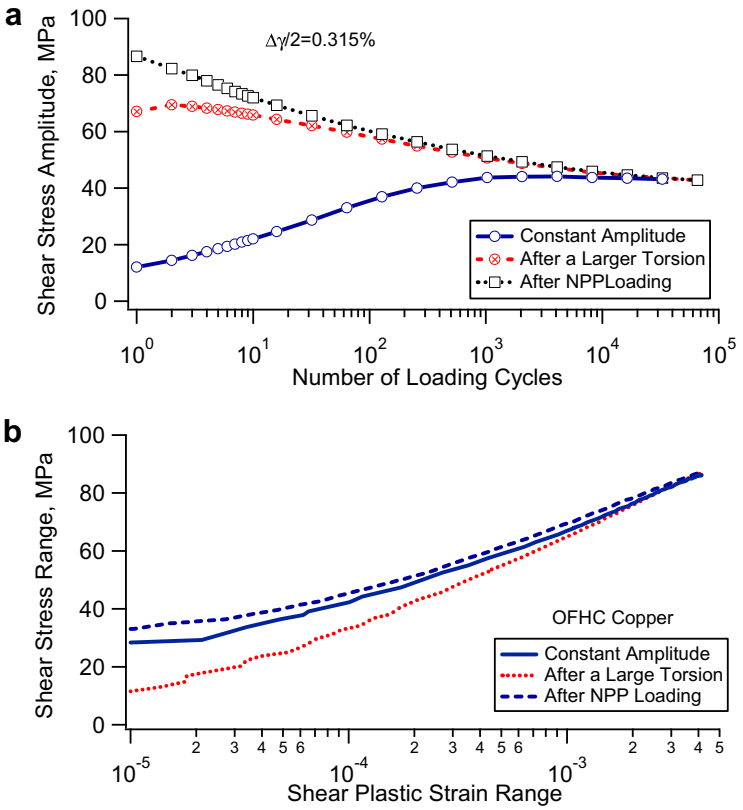


Fig. 14. Reversibility of cyclic plasticity in a textured OFHC copper: (a) shear stress amplitude versus number of loading cycles and (b) shear stress range versus shear plastic strain range (Zhang and Jiang, 2005).

tude in Step 1 were dissociated or converted into irregular persistent slip bands (PSBs) in the Step 2 loading. Under single-step constant amplitude loading at $\Delta\gamma/2 = 0.315\%$, the substructure consisted of dislocation veins and PSBs (Zhang and Jiang, 2005). The difference in substructure may result in the different shape of hysteresis loop.

It should be pointed out that the reversibility of mechanical behavior in a high–low loading sequence can be material dependent. Jiang and Kurath (1997a) experimentally studied the reversibility of plastic deformation of stainless steel 304 under high–low sequence loading. Decreasing step tests were conducted to investigate sequence effects; specially the rate of recoverability for the hardening or softening, and non-Masing deformation. The decreasing loading steps, which allows stable response to occur at a given high constant amplitude before reducing loading level, was conducted to evaluate long-term high–low sequence effects. Fig. 15 illustrates typical results when initial stabilized high level cycling was $\Delta\sigma = 800$ MPa and $\Delta\sigma = 540$ MPa for stainless steel 304. The decreasing step test displayed a marked dependence on prior maximum loading level, even within the context of a final stabilized state. In order to assure that the high loading level in the decreasing step test did not merely alter the initial rate of "recovery" to the stabilized state, several specimens were first stabilized at the higher stress range and then cycled to failure

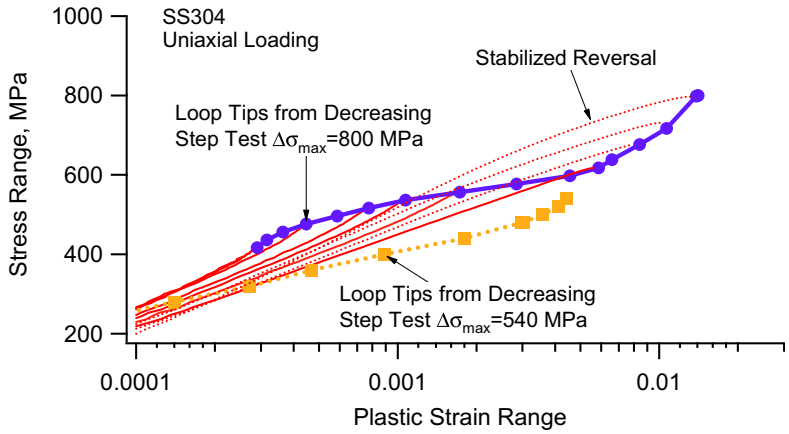


Fig. 15. Experimentally observed sequence dependent cyclic deformation for stainless steel 304 (Jiang and Kurath, 1997a).

at the low level. While the rates tend toward the stabilized state, a migration to the stabilized state continued with additional cycles. In most cases, fatigue failure precluded the return to the stabilized state. For this material, the stress-induced martensite, mechanical twins, and stacking fault may be formed at a high stress amplitude. These structures can be preserved in the subsequent cyclic loading step with a lower stress amplitude, resulting in the irreversibility of stress–strain response.

The experimental results reveal that when a material is subjected to high–low sequence loading, either fully or partial recovery is possible, dependent on the material. The modeling effort by McDowell (1985a) and Ohno (1982) allowed the memory surface to contract in order to capture the possible recovery. Together with the conclusion on the strain range effect and the reversals obtained from the decreasing steps shown in Fig. 15, it can be concluded that the transient behavior under the multiple-step loading cannot be characterized by using the change in the yield stress.

The strain range effect is related to cyclic hardening/softening. If a material displays non-Masing behavior (strain range effect), cyclic hardening will occur when the loading amplitude is switched from a lower level to a higher level. Cyclic softening can be observed when the loading amplitude is decreased from a higher level to a lower level.

## 5. Nonproportional hardening

Nonproportional hardening is the additional hardening behavior of materials under nonproportional loading. Nonproportional hardening has been widely observed on a number of materials (Lamba and Sidebottom, 1978; Kanazawa et al., 1979; Krempl and Lu, 1984; Ohashi et al., 1985; Doong et al., 1990; Khan et al., 2007). 90-degree out-of-phase axial-torsion strain-controlled loading is the most commonly used loading path for studying nonproportional hardening. Krempl and Lu (1984) concluded that, among various nonproportional loading paths, materials subjected to 90-degree out-of-phase axial-torsion loading with a circular path exhibited the highest level of nonproportional hardening.

Nonproportional hardening is material dependent. In face-centered cubic (FCC) alloys, the stacking fault energy (SFE) is an important material parameter that influences the cross-slip of dislocations. The additional hardening (AH) measured from the 90-degree out-of-phase axial-torsion experiments in 316 stainless steel (SFE = 25 MJ/m$^2$, AH = 77%), copper (45 MJ/m$^2$, AH = 35%), and aluminum (135 MJ/m$^2$, AH = 0%) indicates that in the FCC solids solutions, the extra hardening increases with decreasing SFE (Doquet and Clavel, 1996). Carbon steels with body-centered cubic (BCC) crystal structure and high SFE display insignificant nonproportional hardening (Jiang and Kurath, 1997b). For hexagonal close-packed (HCP) metals and alloys, nonproportional hardening was observed in zircaloy-4 but was not observed in titanium alloy VT9 (Xiao et al., 2001; Shukaev, 2001).

Work has been done to comparatively study the slip patterns and dislocation substructures under proportional loading and nonproportional loading to clarify the mechanism of nonproportional hardening (Doong et al., 1990; Zhang and Jiang, 2005). Generally, nonproportional hardening is ascribed to an increase in slip activity due to the rotation of maximum shear stress plane and the enhancement in latent hardening (Kanazawa et al., 1979; McDowell et al., 1988; Doquet and Pineau, 1990; Xiao and Kuang, 1996; Xiao et al., 2001). When an engineering material with complex microstructure such as stainless steels is used for the investigation for nonproportional hardening, precipitates (Clavel and Feaugas, 1996), stress-induced phase transformation (McDowell et al., 1988), mechanical twins (Cailletaud et al., 1991; Doquet, 1993), and heterogeneous substructures (Bocher et al., 2001) may also contribute to the observed nonproportional hardening. Zhang and Jiang (2005) investigated the influence of texture on nonproportional hardening using a single phase polycrystalline material. It was concluded that nonproportional hardening was the result of enhanced activated slip systems and increased uniform activation of slip systems due to the rotation of maximum shear stress under nonproportional loading.

### 5.1. Nonproportional hardening requires a rational definition

Nonproportional hardening can be defined qualitatively. The traditional method based on the von Mises equivalent stress and the equivalent total strain may misinterpret the result of nonproportional hardening (Jiang and Kurath, 1997b). Definitions of the equivalent stress magnitude and the equivalent plastic strain magnitude were given by Jiang and Kurath (1997b) based on the classic cyclic plasticity theories. The equivalent stress magnitude is the radius of the minimum circle that circumscribes the loading path in the deviatoric stress space (Fig. 16a). The equivalent plastic strain magnitude is the radius of the minimum circle that circumscribes the loading path in the plastic strain space (Fig. 16b). Mathematically, the equivalent stress and the plastic strain concept can be expressed as follows:

$$\bar{\sigma}_{\mathrm{a}} = \min\left\{\max\left\{\sqrt{\frac{3}{2}\left(S_{ij}-S^0_{ij}\right)\left(S_{ij}-S^0_{ij}\right)}\right\}\right\} \tag{1}$$

$$\bar{\varepsilon}^p_{\mathrm{a}} = \min\left\{\max\left\{\sqrt{\frac{2}{3}\left(\varepsilon^p_{ij}-\varepsilon^0_{ij}\right)\left(\varepsilon^p_{ij}-\varepsilon^0_{ij}\right)}\right\}\right\} \tag{2}$$

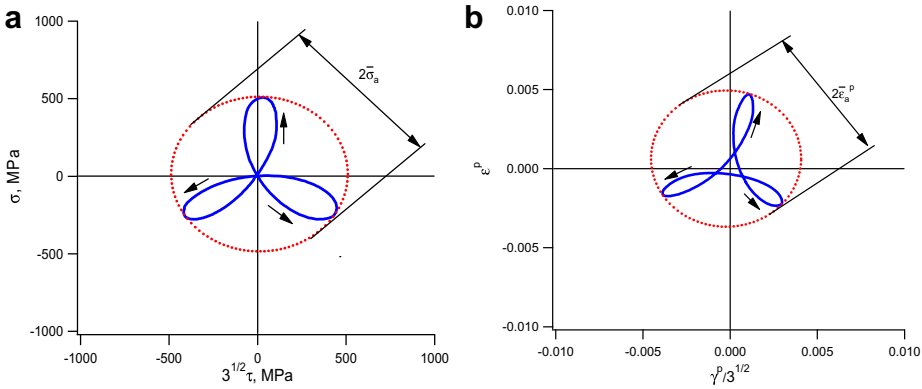


Fig. 16. Definition of equivalent stress magnitude and equivalent plastic strain magnitude: (a) equivalent stress concept and (b) equivalent plastic strain concept.

where $S_{ij}$ are the components of the deviatoric stress, $\varepsilon_{ij}^{p}$ represent the components of the plastic strain. The principle is to find a center of a circle ($S_{ij}^{0}$ or $\varepsilon_{ij}^{0}$) so that the maximum distance to the loading path is a minimum. This minimum distance is the radius of the circle circumscribing the loading path. It is a simple procedure that can be practically implemented computationally. It is noted that a similar definition of equivalent stress was used by Dang Van et al. (1989) for a multiaxial fatigue criterion. The definitions of equivalent stress and plastic strain magnitudes are rooted in the concept of a plastic strain based memory surface to track the loading history. The equivalent plastic strain magnitude after cyclic stabilization is equal to the memory surface size defined by Chaboche et al. (1979).

Fig. 17a shows the simulation results for proportional and nonproportional loading using an Armstrong–Frederick type model (Chaboche et al., 1979) that does not consider nonproportional hardening for stainless steel 304. The axes are the equivalent stress and plastic strain magnitudes (Eqs. (1) and (2)). The nonproportional loading results fall slightly below the proportional results if no additional consideration is made for nonproportional hardening in the Armstrong–Frederick type model. As a general measure of interpreting experimental results, if the experimental results are viewed in terms of the equivalent stress magnitude (Eq. (1)) and the equivalent plastic strain magnitude (Eq. (2)), and the nonproportional data are slightly lower or similar to the proportional data, then nonproportional hardening is minimal or nonexistent. For SS304 stainless steel, nonproportional hardening is minimum at low strain amplitude. However, significant nonproportional hardening occurs at high strain amplitude (Fig. 17b). It is clear that the Armstrong–Frederick type models, such as those of Chaboche et al. (1979), Ohno and Wang (1993), and Jiang and Sehitoglu (1996a) without a special or additional consideration of nonproportional hardening, cannot predict nonproportional hardening.

When a material is subjected to pure shear loading and is followed by tension-compression loading, additional hardening, often referred to as cross-hardening, occurs in the second loading step. Cross-hardening is in fact nonproportional hardening. The results from a specially designed multiple-step loading experiment (Fig. 18) will unmistakably show that *nonproportional hardening is not isotropic behavior.* The tubular specimen made of stainless steel 304 was first subjected to fully reversed pure shear loading with a shear strain amplitude of 0.625% for 4100 loading cycles. The second loading step was a fully

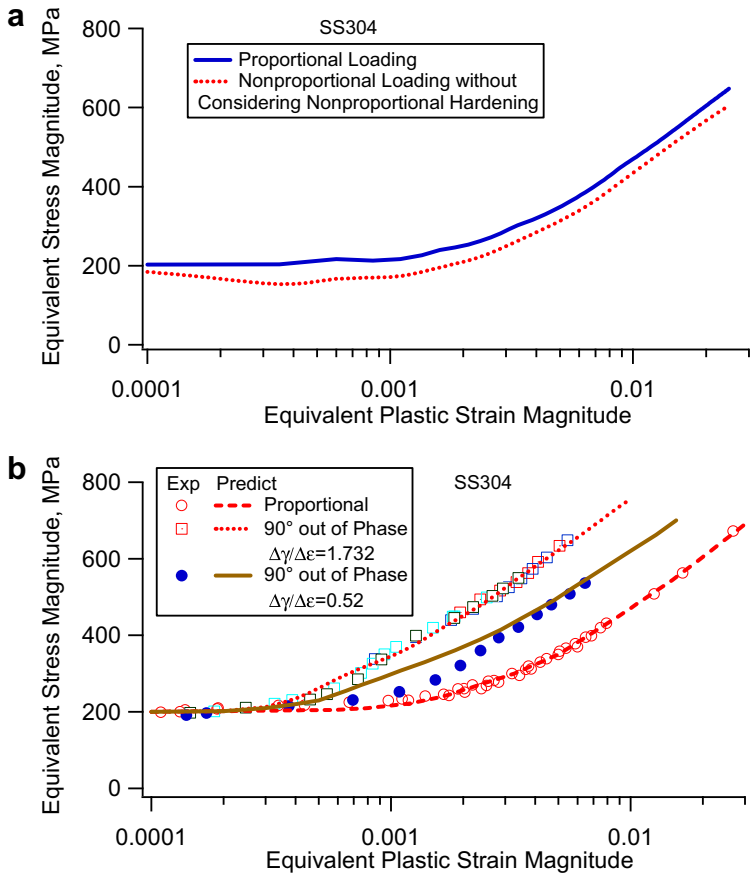


Fig. 17. Comparison of proportional loading history and nonproportional loading history of stainless steel 304 using an Armstrong–Frederick model (Jiang and Kurath, 1997b): (a) without considering additional nonproportional hardening and (b) considering additional nonproportional hardening.

reversed tension-compression with a strain amplitude of 0.36% for 4100 loading cycles. The third step repeated the loading condition of the first loading step. The stress amplitude variations with the number of loading cycles are shown in Fig. 18. The equivalent stress magnitude follows that defined by Eq. (1). Since every loading step was strain-controlled without a mean strain, the loading eliminated ratcheting or stress relaxation phenomenon from influencing the data. The strain amplitudes in all the loading steps were practically identical. Therefore, no strain range effect was introduced. In addition, it should be noticed that the amplitude was incrementally decreased gradually within 20 loading cycles until zero amplitude before the termination of each loading step. Such a gradual decrease in the strain amplitude resulted in zero stress and zero strain at the termination of each loading step. Under the basic framework of cyclic plasticity theories using the yield surface, the decreasing envelope resulted in the yield surface being centered at its origin before the start of the next loading step. The importance for the yield surface to be at the origin will eliminate a possibility to model the observed nonproportional hardening, which will be discussed in a later section.

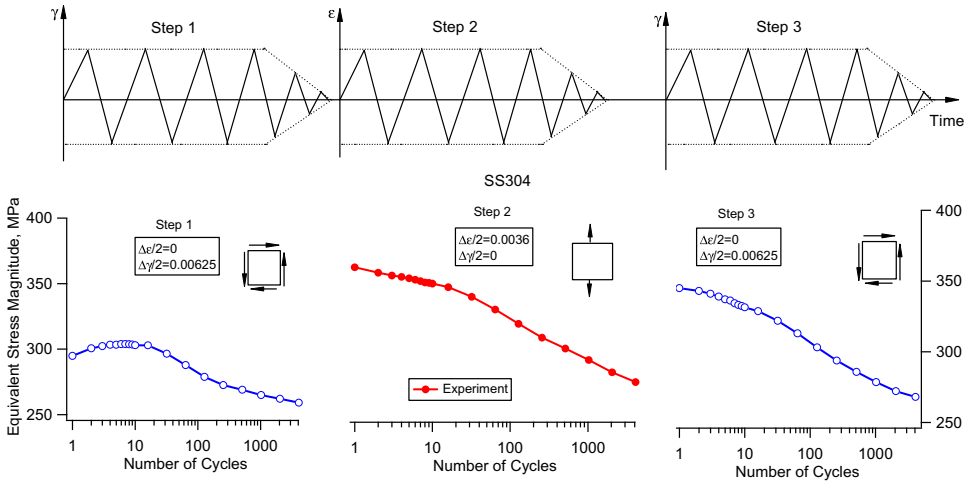


Fig. 18. Variations of stress amplitude with loading cycles for the first three loading steps in a multiple-step loading history of stainless steel 304 (Jiang and Kurath, 1997b).

The results shown in Fig. 18 are the variations of the stress amplitude with loading cycles. The first loading step was pure shear. At a shear strain amplitude of 0.625%, the results suggest that the material displays cyclic softening. This is consistent with the results shown in Fig. 4 obtained from the constant amplitude fully reversed uniaxial tension–compression for the same material. The stress amplitudes in the early part of the second and third loading steps were significantly higher than those obtained from the stabilized constant amplitude loading. Since cyclic hardening and strain range effect are minimal for the material with the identical strain magnitude used in each loading step, the hardening is due to the change in the stress state or the rotation in the maximum shear stress direction between the two consecutive loading steps. The significant higher stress response at the start of the second and third loading steps was the result of nonproportional hardening. The nonproportional hardening was repeatable, indicating that the behavior is not isotropic. Moosbrugger and McDowell (1989) and McDowell (1994) concluded that nonproportional hardening was essentially only of kinematic type for stainless steel 304. McDowell (1985b) showed that a two-surface Mroz-type model can be used for describing nonproportional loading.

Experiments showed that the presence or lack of the decreasing envelope at the end of each loading step had minimal influence on the deformation in the subsequent constant amplitude block. An additional motivation for this type of test is that no definition of equivalent stress or strain is required when interpreting the data.

A similar block loading experiment can be conducted with each loading block consisting of a nonproportional loading step followed by a proportional loading step. If the material displays nonproportional hardening, the stress amplitude in the proportional loading step always decreases with increasing loading cycles. If nonproportional hardening is isotropic behavior, the stress amplitude should be a constant that is much higher than that obtained from a single-step constant amplitude loading with identical loading.

*5.2. The nonproportional hardening cannot be modeled by using the change in the yield stress*

This conclusion is evident by looking at the results obtained from a multiple-step loading history. Fig. 19 shows the stress variation with the number of loading cycles from the first two loading steps of a four-step loading history. The material is pure polycrystalline copper with a grain size of 75 μm. Basic results of the materials can be found in an earlier publication (Zhang and Jiang, 2005). The first loading step was 90-degree out-of-phase strain-controlled axial-torsion loading history with an axial strain amplitude of 0.3% and a shear strain amplitude of 0.52%. The stress response reached a stabilization after 61 loading cycles. Fig. 19a shows the stress amplitude as a function of the loading cycles for Step 1. As can be expected, significant hardening was observed. Before the termination of the first loading cycle, the strain amplitudes were incrementally decreased to zero within 20 loading cycles. The decreasing envelope in the strain amplitudes resulted in practically zero strains and zero stresses at the end of the first loading step.

The second loading step was a pure torsion with a shear strain amplitude of 0.15%. As can be seen from Fig. 19b, significant softening was observed. Stabilization of the stress response can be observed after 160,000 loading cycles in the second loading step. The test was proceeded in the third loading step with identical strain amplitudes to these in the first

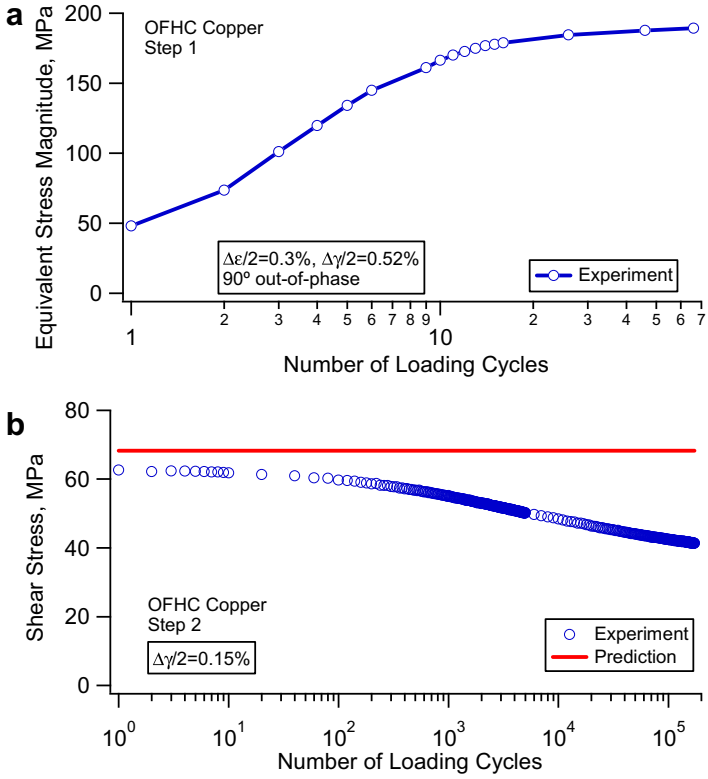


Fig. 19. Stress response obtained from the step loading experiment on OFHC copper; (a) Step 1 (90° out-of-phase axial-torsion, $\Delta\varepsilon/2/2 = 0.3\%$ and $\Delta\gamma/2 = 0.52\%$) and (b) Step 2 (pure torsion, $\Delta\gamma/2 = 0.15\%$).

loading step. Again, the strain amplitudes were incrementally decreased to zero within 20 loading cycles before the end of the third step. The fourth loading step repeated the second loading step in loading mode (pure shear) and number of loading cycles. The specimen did not fail due to fatigue after four loading steps. Significant hardening was observed again in Step 3 and the stabilized stress response was practically identical to that of the first loading step. The stress response in the fourth loading step mimicked that observed in second loading step.

The repeatable stress response in the multiple-step loading further confirms that cyclic hardening and nonproportional hardening are not isotropic behavior. Cyclic hardening/softening is dependent on the loading history. The repeatable stress–strain response in the four-step loading history and the intact specimen suggested that the specimen did not have a fatigue crack that would have influenced the stress–strain response reported for the first two loading steps.

More importantly, the results shown in Fig. 19 reveal that *nonproportional hardening cannot be modeled using the change in the yield stress*. A simple simulation can be conducted based on the Armstrong–Frederick type plasticity models. A closed form solution for the stabilized stress response was derived for the strain-controlled 90-degree out-of-phase axial-torsion loading (Jiang and Kurath, 1996a). The formulas are valid for any plasticity models, such as Chaboche et al. (1979), Ohno and Wang (1993), and Jiang and Sehitoglu (1996a), based on the Armstrong–Frederick basic evaluation rule for the backstress. If an initial yield stress of 11.2 MPa was selected for the pure polycrystalline copper, the yield stress should be 185.6 MPa at the end of the first loading step in order to model the stabilized stress response in the first loading step shown in Fig. 19 by using the increase in the yield stress. The result is practically independent of specific plasticity models as long as the hardening rule is based upon the Armstrong–Frederick dynamic recovery rule and the yield stress is used to characterize nonproportional hardening.

The envelope decrease before the end of the first loading step resulted in the yield surface being centered at the origin of the deviatoric stress coordinates system before the start of the second loading step. With a shear strain amplitude of 0.15% in the second loading step and considering that the material has a shear modulus of 45.5 GPa, any models will predict elastic deformation for the second loading step. This is because the yield stress had to be large enough in order to describe the large stabilized stress response in the first loading step due to nonproportional loading. Elastic deformation is predicted if the shear strain amplitude is less than $k/G$, where $k$ is the yield stress in shear at the end of the first loading step and $G$ is the shear modulus. For the loading case under discussion, $k = 107.2$ MPa (the yield stress was 185.6 MPa), before the start of the torsion loading (Step 2), resulting in $k/G = 0.00236$. In other words, if the shear strain amplitude is less than 0.00236 or 0.236%, any models will predict pure elastic deformation in the second loading step. Clearly, the results shown in Fig. 19b indicate that cyclic plastic deformation occurred in the second loading step despite much lower shear strain amplitude than $k/G$. It should be noted that a very small initial yield stress was used for the material. The discussion is valid if a larger initial yield stress is used.

## 6. Cyclic strain ratcheting

Cyclic strain ratcheting refers to the progressive and directional plastic strain accumulation due to unsymmetrical stress cycling. In the last 20 years, extensive experimental

studies have been conducted on the ratcheting behavior of various metallic materials under both uniaxial and multiaxial loading. Hassan and Kyriakides (1992), Hassan et al. (1992), and Corona et al. (1996) investigated the ratcheting behavior of 1020 and 1026 carbon steels under uniaxial loading and biaxial loading. The effect of the stress amplitude and the mean stress on the ratcheting rate was experimentally studied. Jiang and Sehitoglu (1994a,b) investigated the long-term ratcheting behavior of 1070 steel under proportional, nonproportional, and multiple-step loading conditions. It was found that the ratcheting direction can be different from the mean stress direction dependent on the prior loading history. Significant efforts have been made to experimentally study the effects of the mean stress, the loading amplitude, temperature, loading rate, nonproportional loading path, and alloying on ratcheting strain of stainless steels 304 and 316 (Chaboche and Nouailhas, 1989; Chaboche, 1991; Delobelle et al., 1995; Haupt and Schinke, 1996; Ohno et al., 1998; Kobayashi et al., 1998; Abdel-Karim and Ohno, 2000; Mizuno et al., 2000; Portier et al., 2000; Kang et al., 2002, 2006). For stainless steels, visco-plasticity and dynamic strain aging at elevated temperature have a complex influence on the ratcheting behavior.

Accompanying the extensive experimental studies, significant efforts have been devoted to the development of constitutive models for ratcheting (Chaboche and co-workers, 1979,1986,1991,1994; Voyiadjis and Sivakumar, 1991; Guionnet, 1992; Ohno and Wang, 1993; Hassan and Kyriakides, 1994a,b; Delobelle et al., 1995; McDowell, 1995; Jiang and Sehitoglu, 1996a,b; Ohno, 1997; Xia and Ellyin, 1997; Voyiadjis and Basuroychowdhury, 1998; Bari and Hassan, 2000; Döring et al., 2003; Johansson et al., 2005; Kang et al., 2006). Most of the theories are established on a common framework making use of the yield surface and the translation of the yield surface. A successful approach is to decompose the backstress into several parts and each part is governed by an Armstrong–Frederick type hardening rule. Most of the models were validated using the experimental data from limited or simple experiments. Consequently, most of the constitutive models might predict a special class of ratcheting responses very well, but fail to predict a broader class of ratcheting response (Hassan and Kyriakides, 1994b; Corona et al., 1996; Bari and Hassan, 2000; Bari and Hassan, 2002; Johansson et al., 2005). This section discusses some essential experimental observations which should be considered when developing constitutive models for ratcheting deformation.

### *6.1. Ratcheting rate decay is a common phenomenon*

Fig. 20 shows the stress–strain response of selected loading cycles of three different materials subjected to stress controlled uniaxial loading with non-zero mean stresses. All the three constant amplitude loading experiments were conducted for very long loading cycles. It is noticed that the ratcheting rate, the strain accumulation per loading cycle, decreases with increasing loading cycles for all the three experiments.

Fig. 21 shows the strain response of an experiment on a tubular specimen subjected to a static axial load and fully reversed torsion for 1070 steel. With a static axial load, the fully reversed torsion resulted in ratcheting in the axial direction. The ratcheting rate decreased with increasing loading cycles. Ractheting rate decay was found to be the essential characteristic of strain ratcheting in 1070 steel (Jiang and Sehitoglu, 1994a,b).

A better way to observe ratcheting rate decay is to plot the ratcheting rate against the number loading cycles. Fig. 22 summarize the ratcheting rate results in the form of the ratcheting rate versus the number of loading cycles for four materials under constant ampli-

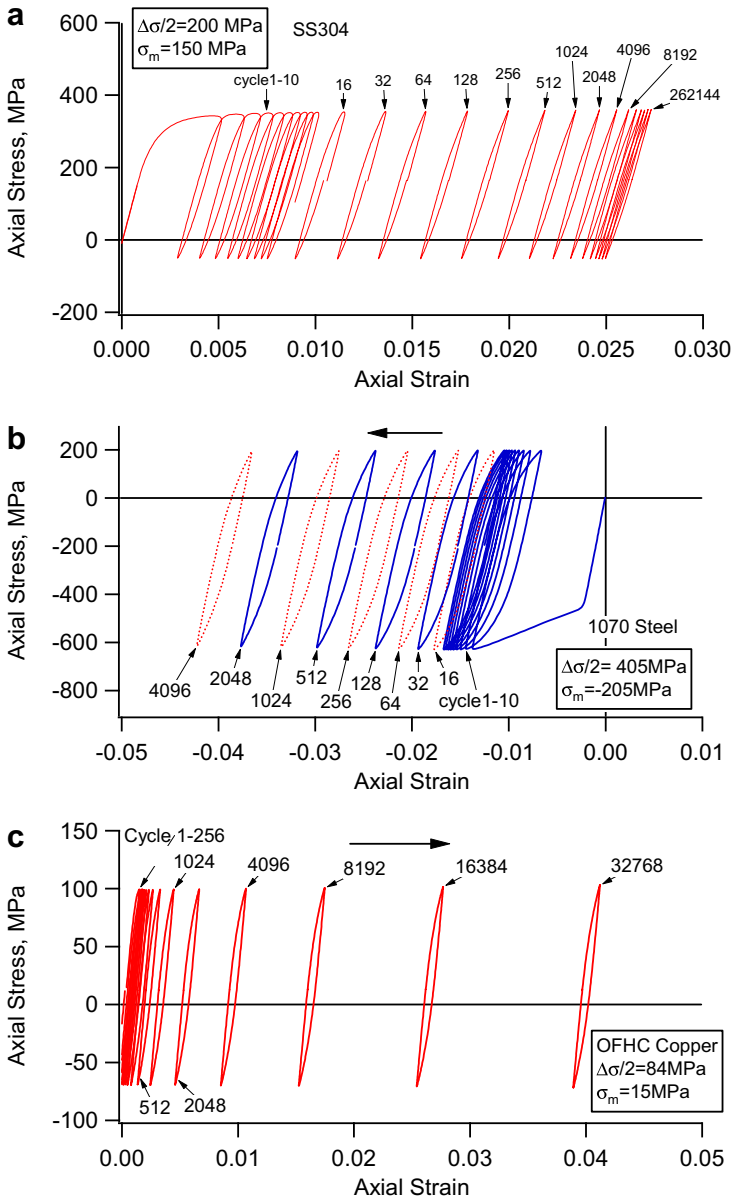


Fig. 20. Cyclic strain ratcheting deformation: (a) stainless steel 304; (b) 1070 steel (Jiang and Sehitoglu, 1994a) and (c) OFHC copper.

tude uniaxial loading. The results from the stainless steel clearly show that the ratcheting persists although the ratcheting rate can be extremely small after over 200,000 loading cycles. Since logarithmic scales are used, the linear curves in Fig. 22 suggest that the ratcheting rate decay approximately follows a power law pattern. It was assumed that the ratcheting rate was approximately constant for 1026 steel (Hassan and Kyriakides, 1992; Hassan et al., 1992). The ratcheting experiments of 1026 steel were conducted for less than

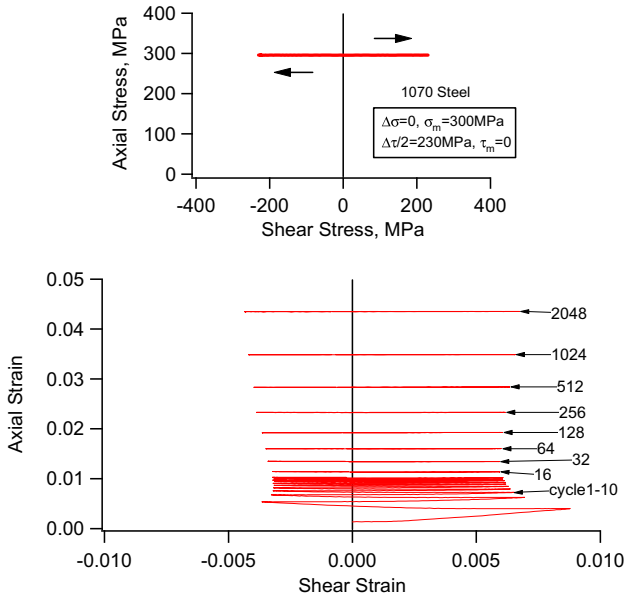


Fig. 21. Strain response of 1070 steel subjected to axial-torsion loading (Jiang and Sehitoglu, 1994a).

100 loading cycles to avoid excessive ratcheting deformation. Reproducing the experimental ratcheting results of two loading cases of 1026 steel in the rate versus number loading cycles format, Fig. 22b clearly shows that the material displays ratcheting rate decay. Near constant rate reported by Hassan and Kyriakides (1992) and Hassan et al. (1992) or ratcheting rate increase was mainly due to the load controlled loading condition. Ratcheting rate is sensitive to the applied stresses. Under a load controlled condition, the applied stress amplitude is increased with the increase in the ratcheting strain.

The power law ratcheting rate decay is general for a number of engineering materials, such as 1045 steel, 1070 steel, and stainless steel 304. The speed of the decay is material dependent and loading magnitude dependent. A theoretical evaluation can be made on any constitutive relation designed for predicting ratcheting based on the general ratcheting rate decay phenomenon. A model should possess the capability to produce power law ratcheting rate decay.

### *6.2. Ratcheting behavior is influenced by prior loading history*

The ratcheting direction can be different from the mean stress direction. To discuss this point, multiple-step loading is required.

Fig. 23 shows the stress–strain response from a two-step tension–compression loading. The first step was a monotonic loading case with a maximum strain being 4.5%. The subsequence loading was under stress control with a stress amplitude of 420 MPa and a mean stress of 100 MPa. It can be found that with a positive mean stress in Step 2, the strain ratcheting followed a negative direction.

The influence of the prior loading history on strain ratcheting can be further found from the following two-step uniaxial experiment shown in Fig. 24. In both steps, the stress

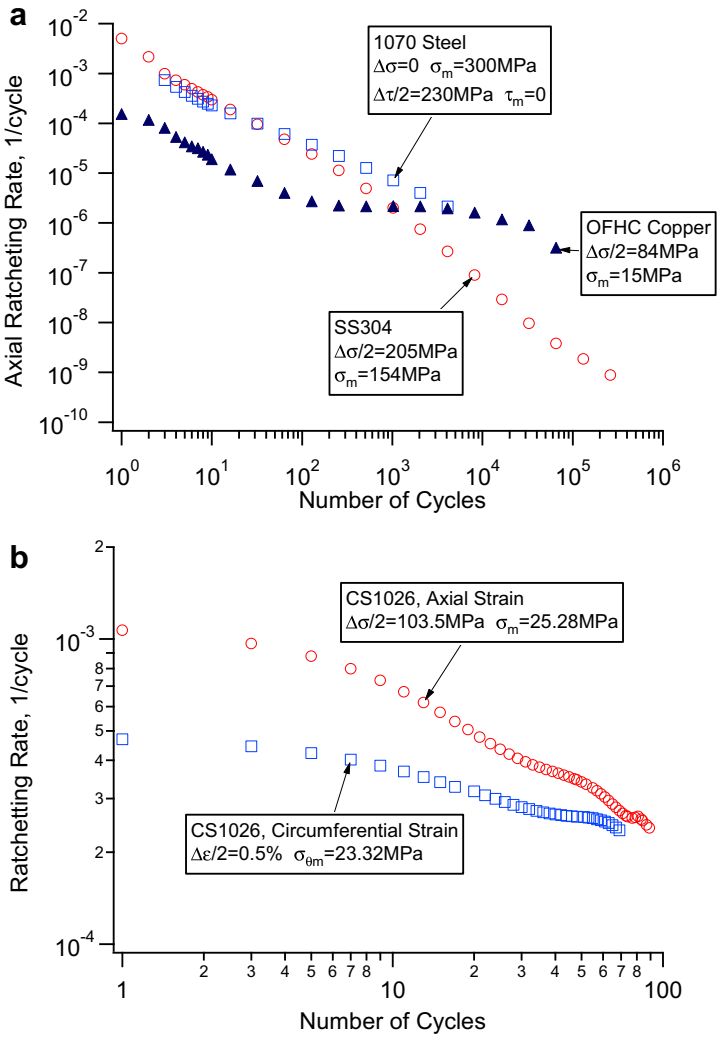


Fig. 22. Ratcheting rate as a function of the number of loading cycle under constant amplitude loading: (a) stainless steel 304 (Fig. 20a); 1070 steel (Fig. 21); and OFHC copper (Fig. 20c) and (b) 1026 steel (Hassan and Kyriakides, 1992; Hassan et al., 1992).

amplitude was 403 MPa. The mean stress in Step 1 was 208 MPa, and the mean stress in Step 2 was 78 MPa. After 4100 loading cycles in Step 1, the test was switched to Step 2. As was expected, the ratcheting direction was consistent with the mean stress direction in Step 1. However, with the positive mean stress in Step 2, the ratcheting direction was opposite to the mean stress direction.

### *6.3. Ratcheting rate decay is not due to the isotropic behavior of the material*

Fig. 25 shows the stress–strain response of selected loading cycles from two consecutive loading steps in a six-step uniaxial ratcheting experiment. The stress amplitude of 382 MPa

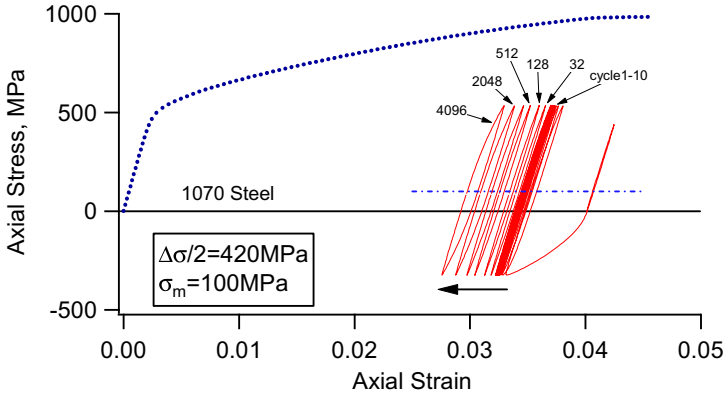


Fig. 23. Cyclic ratcheting of 1070 steel after monotonic tension (Jiang and Sehitoglu, 1994b).

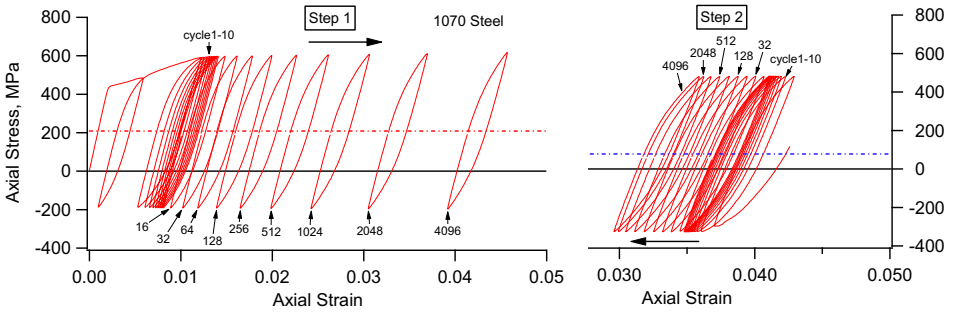


Fig. 24. Cyclic ratcheting deformation of 1070 steel under two-step loading (Jiang and Sehitoglu, 1994b).

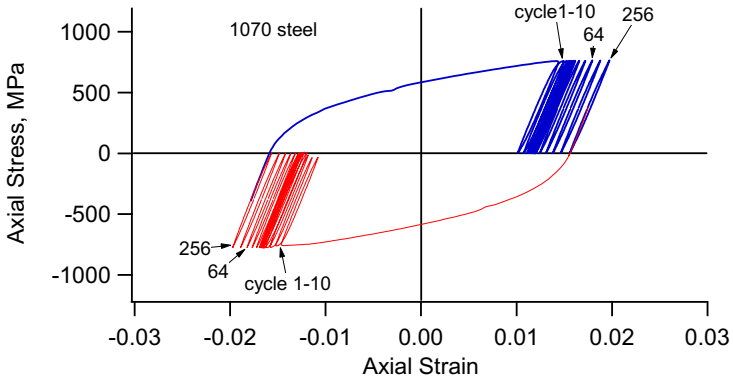


Fig. 25. Cyclic strain ratcheting of 1070 steel in two consecutive loading steps under block loading (Jiang and Sehitoglu, 1994b).

and the value of the mean stress were identical in each loading step. However, the sign of the means stress was opposite in the two consecutive loading steps with positive mean stress for the first loading step. The results shown in Fig. 25 were taken from Step 5

and Step 6. It was found that the ratcheting deformation after the first loading step was practically identical if not considering the sign of the ratcheting strain. Ratcheting rate decayed in every loading step. Such a property suggests that the ratcheting rate decay is not a result of the material's isotropic behavior and it cannot be modeled using an isotropic hardening model. This is because if ratcheting rate decay is caused by the isotropic hardening of the material, there will be no further ratcheting in the subsequent loading steps after the material has been experienced sufficient loading cycles in the first loading step.

### 6.4. Separate material hardening is associated with ratcheting rate decay

It is material's hardening behavior that results in the observed ratcheting rate decay. However, the hardening could be any hardening discussed earlier or a combination of a few types of hardening. The experiments on 1070 steel reveal that none of the hardening discussed so far is essential for ratcheting rate decay. Clearly, nonproportional hardening is not a necessary condition for ratcheting rate decay because ratcheting rate decay occurs under uniaxial loading. Cyclic hardening is not a necessary condition for a material to display ratcheting rate decay because a material, such as 1070 steel, displaying no cyclic hardening, is observed to exhibit significant ratcheting rate decay.

To facilitate a discussion, the hardening associated with the ratcheting rate decay is referred to as ratcheting hardening. Ratcheting hardening can be better viewed by the plot with the stress range versus the plastic strain range. Fig. 26 shows such a plot for 1070 steel subjected to uniaxial loading with a compressive mean stress. The plot is a reproduction of the results shown in Fig. 20b. In the semi-log scale, the branches of the stress–plastic strain hysteresis loops are approximately linear for the loading amplitude and material under consideration. With increasing loading cycles, the slopes of the branches in the semi-log scale increased, resulting in decreased plastic strain ranges. The observed ratcheting rate decay is associated with the change in the slope of the hysteresis loop branches. Again, it should be kept in mind that 1070 steel does not display any significant cyclic hardening.

The branches of the hysteresis loops shown in Fig. 26 exhibit a fan shape. If again an offset of $10^{-4}$ plastic strain range is used to define the yield stress, it is clear that the yield

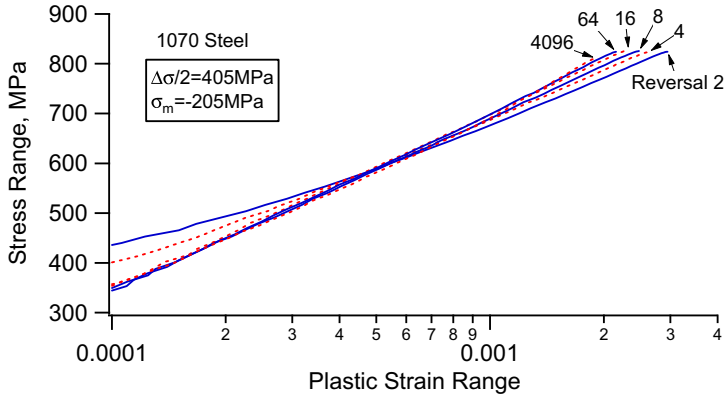


Fig. 26. Reversals during ratcheting deformation of 1070 steel (data identical to that in Fig. 20b).

stress decreased rapidly in the first few loading cycles. Such an observation suggests that the yield stress cannot be used to model the ratcheting rate decay.

It is noticed that for the loading case shown in Figs. 26 and 20b, the ratcheting rate was in the order of $10^{-3}$/cycle for the first few loading cycles. The rate was decreased to approximately $3 \times 10^{-6}$/cycle after 4100 loading cycles. The change in the ratcheting rate is three orders of magnitude. However, the degree of material hardening that has resulted in the significant ratcheting rate decay, as shown in Fig. 26, is not as obvious as that reflected in the ratcheting rate. Such a nature of detailed deformation and the significant change in the ratcheting rate makes accurate modeling of ratcheting rate very difficult.

While ratcheting hardening is a separate material property, it should be noted that cyclic hardening and nonproportional hardening can also contribute to the observed ratcheting rate decay.

## 7. Further discussion

The discussion is concentrated on the macroscopic cyclic plasticity material behavior and engineering modeling of cyclic plasticity, although the experimental results are meaningful to modeling at any material scales. The typical cyclic plasticity behavior can serve as the guideline for a critical evaluation of the plasticity theories. Early plasticity theories often make use of the isotropic hardening and the change in the yield stress to consider the hardening behavior in cyclic plasticity. Clearly, such theories are not appropriate for the description of the general cyclic plasticity deformation.

Most cyclic plasticity theories share the same basic framework using a yield surface in the deviatoric stress space. The normality flow rule is used. The kinematic hardening is considered through the translation of the yield surface and the isotropic hardening is modeled through the extension and contraction of the yield surface. The models differ mainly in the specification of the translation of the yield surface, which is often called the hardening rule.

Based on the hardening rules used, most existing cyclic plasticity models can be classified into two types: Mróz type of models and Armstrong–Frederick type models. In a critical theoretical evaluation (Jiang and Kurath, 1996b), the Mróz type of models were proven to possess mathematical difficulties in dealing with nonproportional loading, in addition to other inferior properties. On the other hand, the Armstrong–Frederick type models possess features that may allow for a proper description of all the cyclic plasticity phenomena discussed in the previous sections upon further refinement.

Based upon the discussion of the results presented in the previous sections, it can be concluded that the consideration of the strain range effect using a memory surface, which was first introduced by Chaboche et al. (1979) and further modified by McDowell (1985a,b) and Ohno (1982), is a correct concept. The detailed modeling of the cyclic hardening and strain range effect should incorporate the dependence of the other material constants than the yield stress alone. An attempt was made in this direction by Jiang and Kurath (1997a) to describe cyclic hardening.

The results shown in Fig. 18 for the nonproportional hardening indicate that the nonproportional hardening is a memory effect instead of instantaneous response. Therefore, the methods, such as those by Benallal and Marquis (1987a,b) and Benallal et al. (1989), making use of an angle between the stress increment and the normal cannot

account for the experimentally observed stress–strain response shown in Fig. 18. This is because the incremental decreasing amplitude used at the end of each loading step brought the yield surface to the origin. The angle used to measure the nonproportionality in such models is always zero in each loading step shown in Fig. 18. As a result, no nonproportional hardening will be predicted. As shown by Jiang and Kurath (1997b), the fourth tensor introduced by Tanaka and Okuchi (1988) and Tanaka (1994) is promising for the consideration of nonproportionality. Since again the change in the yield stress is not appropriate for the consideration of the nonproportional hardening, a model considering the dependence of the material constants in an Armstrong–Frederick hardening rule by Döring et al. (2003) is promising.

Accurate modeling of ratcheting deformation is still a difficult task particularly if the long-term ratcheting is considered. For stable materials which do not display significant nonproportional hardening and cyclic hardening, an Armstrong–Frederick type model by Ohno and Wang (1991) and Jiang and Sehitoglu (1996a) can capture the essential characteristic of ratcheting in terms of ratcheting rate decay and the dependence of ratcheting direction on the prior loading history.

It should be pointed out that the discussion is on "idealized" materials which can be considered to be uniform and initially isotropic. Most materials in engineering applications particularly for those loading bearing components are rolled or forged or machined. The materials are not initially isotropic. Significant texture and residual stresses can be introduced due to the manufacturing processes. Additional considerations of texture, microstructure, and preloading history are needed (Beyerlein and Tome, 2007; Zhang et al., 2007).

The accuracy of modeling is dependent on the particular application. The discussion presented in the article is for a general consideration. Engineering generally aims at a practical solution with a reasonable accuracy. For example, isotropic hardening is a "bad" idea for cyclic plasticity modeling. However, for the modeling of manufacturing process, simplification is necessary and modeling with the isotropic hardening concept could be an acceptable practice at least for the time being.

## 8. Concluding remarks

A careful observation of the results from the cyclic deformation experiments suggests that isotropic hardening is not a major cyclic plasticity property. The change in the yield stress cannot be used to model any cyclic plasticity phenomena.

The results obtained from a well-planed multiple-step experiment can provide cyclic plasticity properties that cannot be explored from regular single-step constant amplitude loading experiments. The experimental phenomena presented in the current article are general for most engineering materials and they should be taken into consideration before developing or revising a cyclic plasticity model.

## Acknowledgement

The experimental results presented in this article were obtained from the research projects supported by the National Science Foundation (CMS-9984857), the Office of Navel Research (N000140510777), and National Natural Science Foundation of China (NSFC) through the Joint Research Fund for Overseas Chinese Young Scholars (50428504).

## References


Abdel-Karim, M., Ohno, N., 2000. Kinematic hardening model suitable for ratcheting with steady-state. Int. J. Plasticity 16, 225–240.

Bari, S., Hassan, T., 2000. Anatomy of coupled constitutive models for ratcheting simulations. Int. J. Plasticity 16, 381–409.

Bari, S., Hassan, T., 2002. An advancement in cyclic plasticity modeling for multiaxial ratcheting simulation. Int. J. Plasticity 18, 873–894.

Benallal, A., Cailletaud, G., Chaboche, J.L., Marquis, D., Nouailhas, D., Rousset, M., 1989. Description and modeling of non-proportional effects in cyclic plasticity. In: Brown, M.W., Miller, K.J. (Eds.), Biaxial and Multiaxial Fatigue, EGF 3. Mechnical Engineering Publication, London, pp. 107–129.

Benallal, A., Marquis, D., 1987a. Constitutive equations for nonproportional elastio-viscoplasticity. ASME J. Eng. Mater. Technol. 109, 326–336.

Benallal, A., Marquis, D., 1987b. Constitutive equations describing nonproportional effect in cyclic plasticity. In: Sedai et al. (Eds.), Proceedings of Second International Conference on Constitutive Laws for Engineering Material: Theory and Applications, Tucson, AZ, pp. 505–512.

Beyerlein, I.J., Tome, C.N., 2007. Modeling transients in the mechanical response of copper due to strain path changes. Int. J. Plasticity 23, 640–664.

Bocher, L., Delobelle, P., Robinet, P., Feaugas, X., 2001. Mechanical and microstructural investigations of an austenitic stainless steel under non-proportional loadings in tension–torsion internal and external pressure. Int. J. Plasticity 17, 1491–1530.

Boller, C., Seeger, T., 1987. Materials Data for Cyclic Loading, Part B: Low-alloy Steels. Elsevier, New York.

Cailletaud, G., Doquet, V., Pineau, A., 1991. Cyclic multiaxial behaviour of an austenitic stainless steel: microstructural observations and micromechanical modeling. In: Kussmaul, K., McDiarmid, D., Socie, D. (Eds.), Fatigue under Biaxial and Multiaxial Loading, ESIS10. Mechanical Engineering Publication, London, pp. 131–149.

Chaboche, J.L., 1986. Time-independent constitutive theories for cyclic plasticity. Int. J. Plasticity 2, 149–188.

Chaboche, J.L., 1991. On some modifications of kinematic hardening to improve the description of ratcheting effects. Int. J. Plasticity 7, 661–678.

Chaboche, J.L., 1994. Modeling of ratcheting: evaluation of various approaches. Eur. J. Mech. A: Solids 13, 501–518.

Chaboche, J.L., Dang Van, K., Cordier, G., 1979. Modelization of the strain memory effect on the cyclic hardening of 316 stainless steel, SMiRT'5, Div. L, Berlin, L 11/3.

Chaboche, J.L., Nouailhas, D., 1989. Constitutive modeling of ratcheting effects. I – experimental facts and properties of the classical models. ASME J. Eng. Mater. Technol. 111, 384–392.

Christ, H.J., Mughrabi, H., 1996. Cyclic stress–strain response and microstructure under variable amplitude loading. Fatigue Fract. Eng. Mater. Struct. 19, 335–348.

Clavel, M., Feaugas, X., 1996. Micromechanisms of plasticity under multiaxial cyclic loading. In: Pineau, A., Cailletaud, G., Lindley, T.C. (Eds.), Multiaxial Fatigue and Design, ESIS 21. Mechanical Engineering Publication, London, pp. 21–41.

Corona, E., Hassan, T., Kyriakides, S., 1996. On the performance of kinematic hardening rules in predicting a class of biaxial ratcheting histories. Int. J. Plasticity 12, 117–145.

Dang Van, K., Griveau, B., Message, O., 1989. On a new multiaxial fatigue limit criterion: Theory and application. In: Brown, M.W., Miller, K.J. (Eds.), Biaxial and Multiaxial Fatigue, EGF 3. Mechanical Engineering Publication, London, p. 749.

Delobelle, P., Robinet, P., Bocher, L., 1995. Experimental study and phenomenological modelization of ratchet under uniaxial and biaxial loading on an austenitic stainless steel. Int. J. Plasticity 11, 295–330.

Doong, S.-H., Socie, D.F., Robertson, I.M., 1990. Dislocation substructures and nonproportional hardening. ASME J. Eng. Mater. Technol. 112, 456–464.

Doquet, V., 1993. Twinning and multiaxial cyclic plasticity of a low stacking-fault energy FCC alloy. Acta Metall. Mater. 41, 2451–2459.

Doquet, V., Clavel, M., 1996. Stacking-fault energy and cyclic hardening of FCC solid solutions under multiaxial nonproportional loadings. In: Pineau, A., Cailletaud, G., Lindley, T.C. (Eds.), Multiaxial Fatigue and Design, ESIS 21. Mechanical Engineering Publication, London, pp. 43–60.

Doquet, V., Pineau, A., 1990. Extra hardening due to cyclic non-proportional loading of an austenitic stainless steel. Scr. Metall. Mater. 24, 433–438.

Döring, R., Hoffmeyer, J., Seeger, T., Vormwald, M., 2003. A plasticity model for calculating stress–strain sequences under multiaxial nonproportional cyclic loading. Comput. Mater. Sci. 28, 596–597.

Fan, Z., Jiang, J., 2004. Investigation of low cycle fatigue behavior of 16MnR steel at elevated temperature. Zhejiang Daxue Xuebao (Gongxue Ban)/Journal of Zhejiang University (Engineering Science) 38, 1190–1195.

Feltner, C.E., Laird, C., 1967a. Cyclic stress–strain response of FCC metals and alloys – I. Phenomenological experiments. Acta Metall. 15, 1621–1632.

Feltner, C.E., Laird, C., 1967b. Cyclic stress–strain response of FCC metals and alloys. II. Dislocation structures and mechanisms. Acta Metall. 15, 1633–1653.

Gao, Z., Zhao, T., Wang, X., Jiang, Y. Multiaxial fatigue of 16MnR steel. ASME J. Pres. Ves. Tech.

Guionnet, C., 1992. Modeling of ratcheting in biaxial experiments. ASME J. Eng. Mater. Technol. 114, 56–62.

Hassan, T., Corona, E., Kyriakides, S., 1992. Ratcheting in cyclic plasticity, Part II: multiaxial behavior. Int. J. Plasticity 8, 117–146.

Hassan, T., Kyriakides, S., 1992. Ratcheting in cyclic plasticity, Part I: uniaxial behavior. Int. J. Plasticity 8, 91–116.

Hassan, T., Kyriakides, S., 1994a. Ratcheting of cyclically hardening and softening materials, I: uniaxial behavior. Int. J. Plasticity 10, 149–184.

Hassan, T., Kyriakides, S., 1994b. Ratcheting of cyclically hardening and softening materials, II: multiaxial behavior. Int. J. Plasticity 10, 185–212.

Haupt, A., Schinke, B., 1996. Experiments on the ratcheting behaviour of AISI 316L (N) austenitic steel at room temperature. ASME J. Eng. Mater. Technol. 118, 281–284.

Heilmaier, M., Maier, H.J., Jung, A., Nganbe, M., Muller, F.E.H., Christ, H.J., 2000. Cyclic stress–strain response of the ODS nickel-base, superalloy PM 1000 under variable amplitude loading at high temperatures. Mater. Sci. Eng. A281, 37–44.

Holzwarth, U., Ebmann, U., 1994. The irreversibility of dislocation-wall formation in persistent slip bands. Phil. Mag. Lett. 70, 75–80.

Jameel, M.A., Peralta, P., Laird, C., 2001. Masing behavior in copper single crystals fatigued under load control. Mater. Sci. Eng. A297, 48–53.

Jiang, Y., 1993. Cyclic plasticity with an emphasis on ratcheting. Ph.D. dissertation, Department of Mechanical Engineering, University of Illinois at Urbana-Champagin.

Jiang, Y., 2001. An experimental study of inhomogeneous cyclic plastic deformation. ASME J. Eng. Mater. Technol. 123, 274–280.

Jiang, Y., 2007. Unpublished experiments results of 1045 steel and stainless steel 304 L.

Jiang, Y., Kurath, P., 1996a. Characteristics of the Armstrong–Frederick type plasticity models. Int. J. Plasticity 12, 387–415.

Jiang, Y., Kurath, P., 1996b. A theoretical evaluation of the incremental plasticity hardening algorithms for cyclic nonproportional loadings. Acta Mech. 118, 213–234.

Jiang, Y., Kurath, P., 1997a. An investigation of cyclic transient behavior and implications on fatigue life estimates. ASME J. Eng. Mater. Technol. 119, 161–170.

Jiang, Y., Kurath, P., 1997b. Nonproportional cyclic deformation: critical experiments and analytical modeling. Int. J. Plasticity 13, 743–763.

Jiang, Y., Sehitoglu, H., 1994a. Cyclic ratcheting of 1070 steel under multiaxial stress states. Int. J. Plasticity 10, 579–608.

Jiang, Y., Sehitoglu, H., 1994b. Multiaxial cyclic ratcheting under multiple step loading. Int. J. Plasticity 10, 849–870.

Jiang, Y., Sehitoglu, H., 1996a. Modeling of cyclic ratcheting plasticity: Part I – development of constitutive equations. ASME J. Appl. Mech. 63, 720–725.

Jiang, Y., Sehitoglu, H., 1996b. Modeling of cyclic ratcheting plasticity: Part II – implement of the new model and comparison of theory with experiments. ASME J. Appl. Mech. 63, 726–733.

Johansson, G., Ekh, M., Runesson, K., 2005. Computational modeling of inelastic large ratcheting strains. Int. J. Plasticity 21, 955–980.

Kanazawa, K., Miller, K.J., Brown, M.W., 1979. Cyclic deformation of 1% Cr–Mo–V steel under out-of-phase loads. Fatigue Eng. Mater. Struct. 2, 217–228.

Kang, G., Gao, Q., Yang, X., 2002. Uniaxial cyclic ratcheting and plastic flow properties of SS304 stainless steel at room and elevated temperatures. Mech. Mater. 34, 145–159.

Kang, G., Kan, Q., Zhang, J., Sun, Y., 2006. Time-dependent ratcheting experiments of SS304 stainless steel. Int. J. Plasticity 22, 858–994.

Kalnaus, S., Jiang, Y., 2007. Multiaxial fatigue of AL6XN stainless steel. ASME J. Eng. Mater. Technol.

Khan, A.S., Kazmi, R., Farrokh, B., 2007. Multiaxial and non-proportional loading responses, anisotropy and modeling of Ti-6Al-4V titanium alloy over wide ranges of strain rates and temperatures. Int. J. Plasticity 23, 931–950.

Kobayashi, M., Ohno, N., Igari, T., 1998. Ratcheting characteristics of 316FR steel at high temperature, part II: analysis of thermal ratcheting induced by spatial variation of temperature. Int. J. Plasticity 14, 373–390.

Krempl, E., Lu, H., 1984. The hardening and rate-dependent behavior of fully annealed AISI Type 304 stainless steel under biaxial in-phase and out-of-phase strain cycling at room temperature. ASME J. Eng. Mater. Technol. 106, 376–382.

Lamba, H.S., Sidebottom, O.M., 1978. Cyclic plasticity for nonproportional paths: Part I – cyclic hardening, erasure of memory, and subsequent strain hardening experiments. ASME J. Eng. Mater. Technol. 100, 96–103.

Li, Y., Laird, C., 1993. Masing behavior observed in monocrystalline copper during cyclic deformation. Mater. Sci. Eng. A161, 23–29.

Maier, H.J., Gabor, P., Gupta, N., Karaman, I., Haouaoui, M., 2006. Cyclic stress–strain response of ultrafine grained copper. Int. J. Fatigue 28, 243–250.

McDowell, D.L., 1985a. A two surface model for transient nonproportional cyclic plasticity, part I: Development of appropriate equations. ASME J. Appl. Mech. 52, 298–302.

McDowell, D.L., 1985b. An experimental study of the structure of constitutive equations for nonproportional cyclic plasticity. ASME J. Eng. Mat. Technol. 107, 307–315.

McDowell, D.L., 1994. Multiaxial effects in metallic materials. Symposium on Durability and Damage Tolerance, ASME AD-Vol. 43, ASME Winter Annual Meeting, Chicago, IL, pp. 213–267.

McDowell, D.L., 1995. Stress state dependence of cyclic ratcheting behavior of two rail steels. Int. J. Plasticity 11, 397–421.

McDowell, D.L., Stahl, D.R., Stock, S.R., Antolovich, S.D., 1988. Biaxial path dependence of deformation substructure of Type 304 stainless steel. Metall. Trans. 19A, 1277–1293.

Metals Reference Book, Third Ed. ASM International, Materials Park (OH), 1993.

Mizuno, M., Mima, Y., Abdel-karim, M., Ohno, N., 2000. Uniaxial ratcheting of 316FR steel at room temperature, part I: Experiments. ASME J. Eng. Mat. Technol. 122, 29–33.

Moosbrugger, J.C., McDowell, D.L., 1989. On a class of kinematic hardening rules for nonproportional cyclic plasticity. ASME J. Eng. Mat. Technol. 111, 87–98.

Ohashi, Y., Tanaka, E., Ooka, M., 1985. Plastic deformation behavior of Type 316 stainless steel subject to out-of-phase strain cycles. ASME J. Eng. Mater. Technol. 107, 286–292.

Ohno, N., 1982. A constitutive model of cyclic plasticity with a nonhardening strain region. ASME J. Appl. Mech. 49, 721–727.

Ohno, N., 1997. Current state of the art in constitutive modeling for ratcheting. Proceedings of the 14th International Conference on SMiRT, Lyon, France, pp. 201–212.

Ohno, N., Abdel-Karim, M., Kobayashi, M., Igari, T., 1998. Ratcheting characteristics of 316FR steel at high temperature: part I: Strain-controlled ratcheting experiments and simulations. Int. J. Plasticity 14, 355–372.

Ohno, N., Wang, J.-D., 1991. Nonlinear kinematic hardening rule with critical state for activation of dynamic recovery. In: Boehler, Khan (Eds.), Proceedings of PLASTICITY'91: Third International Symposium Plasticity and Its Current Applications. Grenoble, France, pp. 455–458.

Ohno, N., Wang, J.-D., 1993. Kinematic hardening rules with critical state of dynamic recovery, part I: Formulations and basic features for ratcheting behavior. Int. J. plasticity 9, 375–390.

Plumtree, A., Abdel-Raouf, H.A., 2001. Cyclic stress–strain response and substructure. Int. J. Fatigue 23, 799–805.

Portier, L., Calloch, S., Marquis, D., Geyer, P., 2000. Ratcheting under tension–torsion loadings: Experiments and modelling. Int. J. Plasticity 16, 303–335.

Pratt, J.E., 1967. Dislocation substructure in strain-cycled copper as influenced by temperature. Acta Metall. 15, 319–327.

Raman, S.G.S., Padmanabhan, K.A., 1996. Effect of prior cold work on the room-temperature low-cycle fatigue behaviour of AISI 304LN stainless steel. Int. J. Fatigue 18, 71–79.

Shukaev, S.N., 2001. Deformation and life of titanium alloy VT9 under conditions of nonproportional low-cycle loading. Strength Mat. 33, 333–338.

Tanaka, E., 1994. A nonproportionality parameter and a cyclic viscoplastic constitutive model taking into account amplitude dependences and memory effects of isotropic hardening. Eur. J. Mech. A: Solids 13, 155.

Tanaka, E., Okuchi, H., 1988. Constitutive modeling of viscoplasticity incorporating nonproportional hardening effects. Trans. JSME Ser. A 54, 1588.

Voyiadjis, G.Z., Basuroychowdhury, I.N., 1998. A plasticity model for multiaxial cyclic loading and ratcheting. Acta Mech. 126, 19–35.

Voyiadjis, G.Z., Sivakumar, S.M., 1991. A robust kinematic hardening rule for cyclic plasticity with ratcheting effects, part I: Theoretical formulation. Acta Mech. 90, 105–123.

Wang, Z., Laird, C., 1988. Relationship between loading process and Masing behavior in cyclic deformation. Mater. Sci. Eng. 101, L1–L5.

Watanabe, C., Kanmuri, K., Kato, M., Onaka, S., Fujii, T., 2002. Rearrangement of fatigue dislocation structure in copper single crystals associated with reduction in the plastic strain amplitude. Phil. Mag. A 82, 1317–1330.

Xia, Z., Ellyin, F., 1997. A constitutive model with capability to simulate complex multiaxial ratcheting behaviour of materials. Int. J. Plasticity 13, 127–142.

Xiao, L., Kuang, Z.-B., 1996. Biaxial path dependence of macroscopic response and microscopic dislocation substructure in Type 302 stainless steel. Acta Metall. 44, 3059–3067.

Xiao, L., Umakoshi, Y., Sun, J., 2001. Cyclic deformation behavior and microstructures of hydrided Zircaloy-4 under biaxial loading. Metall. Mater. Trans. 32A, 2841–2850.

Zhang, J., 2004. Cyclic plastic deformation, fatigue, and associated substructures of polycrystalline copper. Ph.D. dissertation, Department of Mechanical Engineering, University of Nevada, Reno.

Zhang, J., Jiang, Y., 2004. A study of inhomogeneous plastic deformation of 1045 steel. ASME J. Eng. Mater. Technol. 126, 164–171.

Zhang, J., Jiang, Y., 2005. An experimental investigation on cyclic plastic deformation and substructures of polycrystalline copper. Int. J. Plasticity 21, 2191–2211.

Zhang, M., Zhang, J., McDowell, D.L., 2007. Microstructure-based crystal plasticity modeling of cyclic deformation of Ti–6Al–4V. Int. J. Plasticity 23, 1328–1348.